

Traces of urban forest in temperature and CO₂ signals in monsoon East Asia

Keunmin Lee¹, Je-Woo Hong², Jeongwon Kim¹, [Sungsoo Jo¹](#), and Jinkyu Hong¹

¹Department of Atmospheric Sciences, Yonsei University, Seoul, 03722, Korea (Republic of)

²Korea Environment Institute, Sejong, 30147, Korea (Republic of)

Correspondence to: Jinkyu Hong (jhong@yonsei.ac.kr)

Abstract. Cities represent a key space for ~~our~~ sustainable ~~trajectory~~society in a changing environment, and our society is steadily embracing urban green space for its role in mitigating heatwaves and anthropogenic CO₂ emissions. This study reports two ~~year~~ years of surface fluxes of energy and CO₂ ~~measured via the eddy covariance method~~ in an artificially constructed urban forest measured by the eddy covariance method to examine the impact of urban forests on air temperature and net CO₂ exchange. The urban forest site shows typical seasonal patterns of forest canopies with the seasonal march of the East Asian summer monsoon. ~~Our analysis indicates~~ This study shows that the urban forest reduces both the warming trend and urban heat island intensity compared to the adjacent high-rise urban areas and that photosynthetic carbon uptake is large despite relatively small tree density and leaf area index. During the significant drought period in the second year, gross primary production and evapotranspiration decreased, but their reduction was not as significant as those in natural forest canopies. We speculate that forest management practices, such as artificial irrigation and fertilization, enhance vegetation activity. ~~We also stipulate~~ Further analysis reveals that ecosystem respiration in urban forests is more pronounced than for typical natural forests in a similar climate zone. This can be attributed to the substantial amount of soil organic carbon available due to intensive historical soil use and soil transplantation during forest construction, as well as relatively warmer temperatures in urban heat domes. Our ~~observational study also indicates~~ findings suggest the need for caution in soil management ~~for less~~ when aiming to reduce CO₂ emissions in urban areas.

1 Introduction

Cities ~~inhabit~~ make up only 2% of the Earth's land surface but hold more than 55% of the world's population. It is expected that the urban population will reach 68% by 2050 (UN, 2019). With the unprecedented rapid urbanization in the last century, ~~our life trajectory~~ human civilization heavily depends on urban structures and functions, ~~and it is expected that the urban population will increase by up to 68% by 2050 (UN, 2019).~~ Our current Current concern is regarding the disastrous impacts of climatic events (e.g., heatwaves, flooding, and drought) and environmental changes (e.g., air pollution and land degradation) on our socioeconomic system in a changing climate (McCarthy et al., 2010; Rahmstorf and Coumou, 2011). Accordingly, it remains an urgent issue to implement integrated policies for climate change mitigation and adaption toward sustainable cities against global warming and related natural disasters. ~~In particular, urban~~

34 Urban green infrastructures, such as urban ~~forest~~forests, have been recognized as a key solution toward alleviating
35 climatic and environmental disasters (e.g., ~~Oke et al., 2017~~; Chiesura, 2004; Haaland and van den Bosch, 2015;
36 ~~Oke et al., 2017~~; Kroeger et al., 2019). Green spaces in cities, ~~as opposed to gray spaces~~, are exposed to wide
37 ranges of environmental and climatic conditions across geographical locations. Especially when green spaces
38 replace gray infrastructures during ~~the~~-urban redevelopment, it remains unclear whether their benefits emerge in
39 real conditions and thereby ~~outperforming~~overcome their maintenance cost and other harmful effects- (e.g.,
40 allergy and ozone increase). To leverage their full potential benefits, it is necessary to assess the biophysical
41 effects of urban forests based on direct long-term monitoring in urban areas.

42 Urban forests are a key part of green infrastructures in a city, and two of their benefits, which have been mainly
43 addressed in previous studies, are thermal mitigation and carbon uptake (Roy et al., 2012; Oke et al., 2017). Firstly,
44 urban forests mitigate direct sunlight and diminish the incoming radiant energy on the land surface, thereby
45 reducing surface temperature. Additionally, urban forests supply water to the atmosphere through transpiration
46 and retain water for longer ~~times~~-than the impervious surfaces of urban structures. These processes contribute
47 ~~toward~~to reducing air temperature by partitioning more available energy to latent heat flux (Q_E) than sensible heat
48 flux (Q_H), thus creating favorable conditions for mitigating heatwaves and related health problems (e.g., Oke,
49 1982; Hong et al., 2019a). Eventually, this cooling effect reduces the electrical energy load ~~of buildings~~,by air
50 conditioning as well as greenhouse gas emissions. Previous studies have reported cooling effects of urban forests
51 from street trees to parks scales (Oke et al., 1989; Bowler et al., 2010; Norton et al., 2015; Shashua-Bar and
52 Hoffman, 2000). Such cooling effects depend not only on tree species and structures (Feyisa et al., 2014) but also
53 on the size and vegetation density of urban green areas (Yu and Hien, 2006; Chang et al., 2007; Hamada and Ohta,
54 2010; Feyisa et al., 2014). However, despite the strong temperature-controlling factors of evapotranspiration (ET)
55 and ~~direct~~sensible heat fluxes over urban forest canopies, only a few studies have reported on surface energy
56 balance (SEB) in urban forests in relation to thermal mitigation based on direct measurements (e.g., Oke et al.,
57 1989; Spronken-Smith et al., 2000; Coutts et al., 2007a; Ballinas and Barradas, 2015; Hong and Hong, 2016;).
58 Moreover, it is noticeable that forest cooling intensity depends on geography and ~~even~~-forests can even produce
59 a warming trend ~~with the decreased~~as a result of their low albedo (Bonan, 2008; Wang et al., 2018). The lack of
60 direct urban forest measurements hinders proper assessment of their influences on the climate and environment.

61 Furthermore, urban forests mitigate anthropogenic carbon emissions by photosynthetic CO₂ uptake. Traditionally,
62 carbon uptake by urban forests has been estimated by empirical relationships (e.g., biomass allometric equation)
63 or short-term inventory of biomass data and vegetation growth rates, which have limitations of spatiotemporal
64 coverage (Rowntree and Nowak, 1991; Nowak, 1993; Nowak et al., 2008; Weissert et al., 2014). Currently, the
65 eddy covariance (EC) method is being applied in various ecosystems from grasslands and natural forests to urban
66 areas because it provides continuous net CO₂ flux measurements at the neighborhood scale every half hour
67 (Christen 2014). From this perspective, the EC method is useful for studying the net CO₂ exchange (F_c) from
68 diurnal to interannual variations, with its simultaneous measurement of surface energy fluxes. Recently, direct F_c
69 measurements have been performed using the EC method in urban green spaces to examine SEBturbulent
70 exchanges of energy and carbon exchange (Coutts et al., 2007a, 2007b; Awal et al., 2010; Kordowski and Kuttler,

71 [2010](#); Bergeron and Strachan, 2011; Crawford et al., 2011; ~~Kordowski and Kuttler, 2010~~; Peters and McFadden,
72 2012; Velasco et al., 2013; Ward et al., 2013; Ueyama and Ando, 2016; Hong et al., 2019b; ~~Hong et al., 2020~~).
73 However, the EC method provides only the net effects of CO₂ exchange from various carbon sources and sinks,
74 which limits the physical interpretation and assessment of the benefits and costs of urban forests.

75 ~~Flux partitioning into photosynthesis and ecosystem respiration from the EC measured F_C requires additional~~
76 ~~information and data processing (It is [Stoy et al., 2006](#)). It is more~~ challenging to partition F_C into individual
77 sources and sinks, ~~particularly~~ in urban areas because of the complex contributions from biogenic (e.g., vegetation
78 photosynthesis, respiration of vegetation, soil, and humans) and extra anthropogenic (e.g., fossil fuel combustion
79 by transportation or in households and commercial buildings) processes (Pataki et al., 2003). ~~Stochastic F_C~~
80 ~~partitioning methods were recently applied by reprocessing EC observation data with auxiliary data and provided~~
81 ~~useful knowledge on urban~~

82 ~~carbon cycle (Hiller et al., 2011; Crawford and Christen, 2015; Menzer and McFadden, 2017; Stagakis et al.,~~
83 ~~2019).~~

84 With this background, the objectives of this study include: 1) reporting temporal changes in air temperature after
85 the artificial construction of an urban forest park in the Seoul metropolitan area ~~wherewith~~ a hot and humid
86 summer ~~season affects~~ and ~~shows steep global warming trends (Hongcold and Hong, 2016)~~ ~~dry winter seasons~~ and
87 2) quantifying the carbon uptake of urban forests based on ~~the F_C -partitioning through the of F_C~~ data
88 ~~observed~~ ~~measured~~ by the ~~EC~~ Ceddy covariance method and meteorological data (Lee et al., 2021). Here, we
89 highlight the biotic and abiotic factors controlling the carbon cycle in urban forests and the impact of urban forests
90 on the thermal environment after forest park construction.

91 **2 Materials and Methods**

92 **2.1 Urban surface energy and CO₂ balances**

93 The SEB is expressed as:

$$94 \quad Q^* + Q_F = Q_H + Q_E + \Delta Q_S + \Delta Q_A \quad (1)$$

95 where Q^* is the net all-wave radiation of the sum of outgoing and incoming short- and long-wave radiative fluxes,
96 Q_F is the anthropogenic heat flux, Q_H is the turbulent sensible heat flux, Q_E is the latent heat flux, ΔQ_S is the net
97 storage heat flux, and ΔQ_A is the net heat advection (Definitions of variables in Appendix A).

98 The surface CO₂ budget in an urban forest is formulated as follows:

$$99 \quad F_C = E_R + E_B + RE - GPP \equiv E_R + E_B + NBE \quad (2)$$

100 where F_C is the net CO₂ exchange at the city-atmosphere interface, E_R and E_B are the anthropogenic CO₂ emissions
101 from fossil fuel combustion by vehicles and heating in a building, respectively. GPP and RE are biotic
102 contributions to F_C ; GPP is the gross primary production ~~as a result of~~ ~~by~~ photosynthetic CO₂ uptake, and RE is

103 the ecosystem respiration from soil and vegetation. Urban ecosystem respiration considers not only the autotrophic
104 and heterotrophic respirations of vegetation and soil but also human respiration (Moriwaki and Kanda, 2004;
105 Velasco and Roth, 2010; Ward et al., 2013, 2015; Hong et al., 2020). ~~Human respiration is negligible in this study~~
106 ~~because there is no residential population in the park. Vegetation in urban areas includes trees and lawns in urban~~
107 ~~forests, as well as gardens and roadsides, and it offsets CO₂ emissions through CO₂ assimilation by photosynthesis~~
108 ~~as the only carbon sink. Human respiration by park visitor is negligible with 0.4 μmol m² s⁻¹ at most .~~
109 Additionally, *NBE* is the net biome CO₂ exchange and is typically defined as the net ecosystem exchange by *RE*
110 – *GPP* for natural vegetation. Put differently, *NBE* refers to carbon losses in heterotrophic respiration minus the
111 net primary production on natural vegetative surfaces; thus, negative *NBE* indicates the net carbon uptake by the
112 natural ecosystem (Kirschbaum et al., 2001; Randerson et al., 2002). Unlike natural ecosystems, the *F_C* between
113 an urban forest and atmosphere is a complex mixture of biogenic (i.e., *GPP* and *RE*) and anthropogenic (i.e., *E_R*
114 and *E_B*) processes across various spatial and temporal scales. In urban environments, anthropogenic emissions
115 depend on the local characteristics (e.g., ~~transport options, fuel types, heating demand,~~ climate, population density,
116 levels of industrial activity, and existing carbon intensity of electricity supply) of the city ~~and locations of the~~
117 ~~eddy covariance system~~ (Feigenwinter et al., 2012; Kennedy et al., 2014; Lietzke et al., 2015; Stagakis et al.,
118 2019).

119

120 2.2 Site description

121 2.2.1 ~~Seoul Forest Park~~

122 ~~Micrometeorological measurements were taken at the Seoul Forest Park (SFP) in the Seoul metropolitan area,~~
123 ~~Korea (37.5446°N, 127.0379°E). SFP is the third largest park in Seoul with an area of 1.16 km² (Fig. 1a). This~~
124 ~~area had been used as a horse racetrack and a golf course inside the track since 1950 and was surrounded by~~
125 ~~cement factories to the west (Fig. 1b). The local government initially planned this area as a commercial district~~
126 ~~with a high-rise multi-purpose building complex but changed its plan to redevelop the area as a green space in~~
127 ~~late 1990s. The construction of the SFP began in December 2003, and it was opened to the public in June 2005~~
128 ~~(Fig. 1c).~~

129 ~~The dominant land cover within a 300-m radius of the measurement system is a deciduous forest with irrigated~~
130 ~~grass lawns (*Zoysia*), oak (*Quercus acutissima*), ginkgo (*Ginkgo biloba*), and ash trees (*Fraxinus rhynchophylla*),~~
131 ~~which correspond to the Local Climate Zone (LCZ) ‘A’, dense trees (Stewart and Oke, 2012). The maximum leaf~~
132 ~~area index (LAI) of 300 × 300 m² around the SFP tower is approximately 1.6 (Copernicus Service information,~~
133 ~~2020). On the east side (0–120°), there are trees (approximately 230 stems ha⁻¹) with a small artificial lake and~~
134 ~~grasslands beyond it. Trees mainly occupy the southern and western directions of a tower (120–330°) within a~~
135 ~~100-m radius area (approximately 540 stems ha⁻¹) and traffic roads lie outside of the dense vegetation. The mean~~
136 ~~tree height (*h_e*) is approximately 7.5 m and ranges between 5.8–9.5 m. The mean roughness length (*z₀*) and zero-~~
137 ~~plane displacement height (*z_d*) are estimated by the tree height-based approach within 100-m radius and they range~~
138 ~~between 0.3–0.6 and 4.1–8.2 m, respectively (Raupach et al., 1991). *z₀* and *z_d* have seasonal and directional~~

139 ~~variations depending on the variability of the leaves on the vegetation (Lee, 2015; Kent et al., 2018). z_0 and z_d~~
140 ~~change from approximately 0.6 and 5.0 m during leaf-on period (June–August) to 1.2 and 3.0 m during the leaf-~~
141 ~~off periods (December–February) by the Maedonald method (Maedonald et al., 1998). Approximately 80% of the~~
142 ~~footprint area of the SFP tower is within 250 m (Fig. 1e).~~

143 ~~The traffic roads consist of eight and ten lanes carrying heavy traffic throughout the day (~100,000 vehicles day⁻¹)~~
144 ~~to the south and west of the tower (Fig. 1e). Hourly traffic volume, which is used for surface flux partitioning,~~
145 ~~is evaluated on the road adjacent to the SFP tower every year by the Seoul Metropolitan Government~~
146 ~~(<https://topis.seoul.go.kr>). Across the road on the western side of the tower, a cement factory still exists, although~~
147 ~~its size is smaller than it used to be in the past (Fig. 1b and 1e).~~

148 **2.2.2 Climate conditions**

149 Climatic condition shows a distinct seasonal variation with the seasonal march of the East Asian summer monsoon-
150 (Fig. 1). The mean climatological values (1981-2010) of the screen-level air temperature (T_{air}) and precipitation
151 were 12.5°C and 1450 mm year⁻¹, respectively. During the study period (June 2013–May 2015), the observed T_{air}
152 was higher than the climatological mean. Higher temperatures lasted longer in the summer of 2013 with the
153 stagnation of the migratory anticyclones (June) and North Pacific anticyclone (July–August). There were strong
154 heatwaves in the spring seasons of 2014 and 2015 (Hong et al., 2019a). Wind direction also shows seasonal
155 variation with the monsoon system. Main wind comes from vegetative surface in the park, but other land cover
156 types are included differently with seasons. Prevailing wind is southwesterly in spring and summer and changes
157 to northeasterly in autumn and northwesterly in winter (Fig. 2). Accordingly, road fraction in flux footprint is
158 larger in spring and summer and building emission is included only winter season with northeasterly wind (Fig.
159 3f and 2).

160 Notably, seasonal precipitation shows a contrasting pattern between two consecutive years (Fig. 2d1d). In the first
161 year (June 2013–May 2014), annual precipitation was 1256 mm, which corresponded to approximately 90% of
162 the climatological mean. In addition, approximately 50% of the annual rainfall was concentrated in the summer
163 with an estimated 650 mm occurring only in July 2013; however, in the second year the annual rainfall was 932
164 mm (i.e., 67% of the climatological mean) (i.e., the smallest annual precipitation in the past 20 years). The
165 monthly precipitation values in the July and August of 2014 were 198 and 169 mm, respectively, which
166 represented only approximately 35% of the climate mean. Accordingly, the vapor pressure deficit (VPD) and
167 downward shortwave radiation (K_d) in July 2013 were relatively smaller than those in July 2014 (Fig. 2b and 2c).

168 **2.2.2 Seoul Forest Park**

169 Micrometeorological measurements were taken at the Seoul Forest Park (SFP) in the Seoul metropolitan area,
170 Korea (37.5446°N, 127.0379°E). SFP is the third largest park in Seoul with an area of 1.16 km² (Fig. 3a). This
171 area had been used as a horse racetrack and a golf course inside the track since 1950 and was surrounded by
172 cement factories to the west (Fig. 3b). The local government initially planned this area as a commercial district
173 with a high-rise multi-purpose building complex but changed its plan to redevelop the area as a green space in

174 late 1990s. The construction of the SFP began in December 2003, and it was opened to the public in June 2005
175 (Fig. 3c).

176 The mean tree height (h_c) is approximately 7.5 m and ranges between 5.8–9.5 m. Analysis and estimation of
177 roughness elements and integral turbulence characteristics are reported in Kent et al. (2018) and here we explain
178 the key information. 1-m horizontal resolution digital terrain and digital surface model data are analyzed for
179 roughness parameters and tree heights. The mean roughness length (z_0) and zero-plane displacement height (z_d)
180 range between 0.3–0.6 and 4.1–8.2 m with wind directions, respectively. z_0 and z_d have seasonal and directional
181 variations depending on the variability of the leaves on the vegetation (Lee, 2015; Kent et al., 2018). z_0 and z_d
182 change from approximately 0.6 and 5.0 m during leaf-on period (June–August) to 1.2 and 3.0 m during the leaf-
183 off periods (December–February).

184 Approximately 80% of the footprint area of the SFP tower is within 250 m (Fig. 3e) and the dominant land
185 cover within this range is a deciduous forest with irrigated grass lawns (*Zoysia*), oak (*Quercus acutissima*),
186 ginkgo (*Ginkgo biloba*), and ash trees (*Fraxinus rhynchophylla*), which correspond to the Local Climate
187 Zone (LCZ) ‘A’, dense trees (Stewart and Oke, 2012). The maximum leaf area index (LAI) of $300 \times 300 \text{ m}^2$
188 around the SFP tower is approximately 1.6 (Copernicus Service information, 2020). On the east side (0–
189 120°), there are trees (approximately $230 \text{ stems ha}^{-1}$) with a small artificial lake and grasslands beyond it.
190 **2.2.3 Observations in the Seoul Metropolitan Area**

191 In this study, meteorological data from six stations (one eddy covariance station, one aerodrome meteorological
192 observation station, and four automatic weather stations) in the Seoul Metropolitan Area are additionally analyzed
193 to examine the heat mitigation and CO₂ reduction effects of urban vegetation in the SFP (Table 1 and Fig. 1a).
194 The Eunpyeong eddy covariance site (EP, 37.6350°N, 126.9287°E) is for surface flux observations in the
195 northwest of Seoul, where there was a recent urban redevelopment to high-rise and high population residential
196 areas from low-rise areas (Hong and Hong, 2016; Hong et al., 2019b). Flux observations at the site have been
197 conducted since 2012, and they show the SEB and turbulence characteristics of a typical urban residential area.
198 Because the area around the SFP was originally planned to be redeveloped to high-rise high-population residential
199 buildings, EP is selected for comparative analysis as a hypothetical place for the SFP region because they are
200 close to each other and so have the similar synoptic conditions.

201 The Gimpo Airport Observatory (GP, 37.5722°N, 126.7751°E) is located on the western boundary of Seoul, and
202 it is surrounded by grasslands and croplands, which corresponds to LCZ ‘D’. As the dominant wind comes from
203 the west, the GP site is generally affected by the same synoptic weather conditions as Seoul. The GP station
204 represents the rural environment of the Seoul Metropolitan Area because urban development is restricted around
205 the airport (Hong et al., 2019a). In this study, we select the GP site as a reference point and calculate the urban
206 heat island intensity (UHI) as the synchronous difference in T_{air} between the urban and rural areas accordingly
207 (Stewart, 2011).

208 The Seongdong Observatory (SD, 37.5472°N, 127.0389°E), the closest station to the SFP, is located
209 approximately 300 m north of the SFP tower (Fig. 1c). Since the station began observations in August 2000, the
210 meteorological data at SD are useful for analyzing temperature changes before and after the construction of the

211 ~~SFP. Accordingly, it is used to analyze local climatic changes caused by the SFP. Moreover, SD provides auxiliary~~
212 ~~weather variables (e.g., precipitation) that are not observed in SFP station and reference data for surface flux gap~~
213 ~~filling. The Gangnam, Seocho, and Songpa observatories (hereafter denoted as AVG) are located in Seoul's~~
214 ~~central business district, which corresponds to LCZ 1 or 2. These sites are also close to the SFP (~5 km); thus,~~
215 ~~temperatures in these regions can be assumed to be exposed to the same synoptic condition. These regions show~~
216 ~~greater UHI than other parts of Seoul because of dense skyscrapers, according to the analysis of the spatial~~
217 ~~distribution of UHI in Seoul (Hong et al., 2013). The average temperature of these three automatic weather~~
218 ~~stations is used to evaluate the temperature and UHI reduction effects of the SFP construction. All meteorological~~
219 ~~data from the automatic weather station and aerodrome meteorological observation station are observed every~~
220 ~~minute, and they are averaged for 1 h for UHI analysis. All the meteorological data are processed for quality~~
221 ~~control on the National Climate Data Portal of the Korea Meteorological Administration (<http://data.kma.go.kr>).~~

222 **2.3 Instrumentation and data processing**

223 Trees mainly occupy the south and west sectors of a tower (120–330°) within a 100-m radius area (approximately
224 540 stems ha⁻¹) and traffic roads lie outside of the park (Fig. 3f).

225 The measurement system was installed on the rooftop of the SFP facility building (Fig. 4d3d). A three-dimensional
226 sonic anemometer (CSAT3A, Campbell Scientific, USA) and enclosed infrared gas analyzer (EC155, Campbell
227 Scientific, USA) were mounted 12.2 m above the ground level (2.8 m above the roof of an 8.4 m high building)
228 in June 2013 for 2 years (Fig. 4d3d). The eddy covariance data were recorded using the data logger (CR3000,
229 Campbell Scientific, USA) with a 10-Hz sampling rate and a 30-min averaging time. The gas analyzer was
230 calibrated with standard CO₂ gas every three months. ~~The main footprint covered the forest canopies, and the~~
231 The
232 measurement height (z_m) satisfied the tower height requirement over forested or more structurally complex
233 ecosystems in most of wind directions (i.e., $z_m \cong z_d + 4(h_c - z_d)$) (and turbulent flow is in the skimming flow
234 region (Grimmond and Oke, 1999; Munger et al., 2012; Kent et al., 2018). Two radiometers (NR Lite2 and CMP3,
235 Kipp&Zonen, Netherlands) were used to measure the radiative fluxes. An auxiliary measurement included a
236 humidity and temperature probe (HMP155A, Vaisala, Finland) and EVI (Enhanced Vegetation Index) by in situ
LED sensors.

237 ~~The 30-min flux is~~The roads consist of eight and ten lanes carrying heavy traffic throughout the day (~100,000
238 vehicles day⁻¹) to the south and west of the tower (Fig. 3c). Hourly traffic volume, which is used for surface flux
239 partitioning, is evaluated on the road adjacent to the SFP tower every year by the Seoul Metropolitan Government
240 (<https://topis.seoul.go.kr>). Across the road on the western side of the tower, a cement factory still exists, although
241 its size is smaller than it used to be in the past (Fig. 3b and 3c).

242 **2.2.3 Observations in the Seoul Metropolitan Area**

243 Meteorological data from six stations (one eddy covariance station, one aerodrome meteorological observation
244 station, and four automatic weather stations) in the Seoul Metropolitan Area are analyzed to examine the heat
245 mitigation and CO₂ reduction effects of urban vegetation in the SFP (Table 1 and Fig. 3a). The Eunpyeong eddy

246 covariance site (EP, 37.6350°N, 126.9287°E) is for surface flux observations in the northwest of Seoul, where
247 there was a recent urban redevelopment to high-rise and high-population residential areas from low-rise areas
248 (Hong and Hong, 2016; Hong et al., 2019b). Flux observations at the site have been conducted since 2012, and
249 they show the surface energy fluxes and turbulence characteristics of a typical urban residential area. Because the
250 area around the SFP was originally planned to be redeveloped to high-rise high-population residential buildings,
251 EP is selected for comparative analysis as an antipodal place for the SFP region because the sites are close to each
252 other and so have the similar synoptic conditions.

253 The Gimpo Airport weather station (GP, 37.5722°N, 126.7751°E) is located on the western boundary of Seoul,
254 and it is surrounded by grasslands and croplands, which corresponds to LCZ 'D'. As the dominant wind comes
255 from the west, the GP site is generally affected by the same synoptic weather conditions as Seoul. The GP station
256 represents the rural environment of the Seoul Metropolitan Area because urban development is restricted around
257 the airport. In this study, we select the GP site as a reference point and calculate the urban heat island intensity
258 (UHI) as the synchronous difference in T_{air} between the urban and rural areas accordingly (Stewart, 2011).

259 The Seongdong weather station (SD, 37.5472°N, 127.0389°E), the closest station to the SFP, is located
260 approximately 300 m north of the SFP tower (Fig. 3c). Since the station began observations in August 2000, the
261 meteorological data at SD are useful for analyzing temperature changes before and after the construction of the
262 SFP. Accordingly, it is used to analyze local climatic changes caused by the SFP. Moreover, SD provides auxiliary
263 weather variables (e.g., precipitation) that are not observed in SFP station and reference data for the gap filling.

264 The Gangnam, Seocho, and Songpa weather stations (hereafter denoted as CBD) are located in Seoul's central
265 business district, which corresponds to LCZ 1 or 2. These sites are also close to the SFP (~ 5 km); thus,
266 temperatures in these regions can be assumed to be exposed to the same synoptic condition. The annual mean
267 maximum UHI of CBD ranges from 3.7 to 5 °C and is similar to that of the SD. These regions show greater UHI
268 than other parts of Seoul because of dense skyscrapers (Hong et al., 2013; Hong et al., 2019a). The average
269 temperature of these three automatic weather stations is used to evaluate the temperature and UHI reduction
270 effects of the SFP construction. All meteorological data from the automatic weather station and aerodrome
271 meteorological observation station are observed every minute, and they are averaged for 1 h for UHI analysis.
272 All the meteorological data are processed for quality control on the National Climate Data Portal of the Korea
273 Meteorological Administration (<http://data.kma.go.kr>).

274 **2.3 Data processing procedures**

275 Turbulent fluxes are computed using EddyPro (6.2.0 version, LI-COR), with the applications of the double
276 rotation, time lag compensation using covariance maximization, ~~spike removal and~~ quality test (~~Vickers, and~~
277 ~~Mahrt, 1997~~), spectral corrections ~~for low frequency (Monerieff(Hong et al., 2004) and high frequency (Fratini~~
278 ~~et al., 2012), as well as vertical sensor separation correction (Horst and Lenschow, 2009)2020 and references~~
279 ~~therein~~). We apply the following post processes for quality control: 1) plausible value check, 2) spike removal,
280 and 3) discarding the negative F_C flux during the nighttime (*i.e., no photosynthesis at night*) (Hong et al., 2020).

281 The total study period from installation (31 May, 2013) to termination (03 June, 2015) is approximately 2 years
282 (35,174 potential 30-min data), and ~~the~~in December 2013, there was a gap for approximately 4 weeks due to the
283 power system failure. The total available data are approximately 90.1%, 88.3%, and 85.4% ($n = 31709, 31064,$
284 30028) for Q_H , Q_E , and F_C ~~after the processes~~, respectively.

285 The flux partitioning and gap filling methods are well documented in previous studies of Lee et al. (2021) and
286 Hong et al. (2019b) and here we describe the core of the methods. Missing values in turbulent exchange of energy
287 and CO_2 are filled with an artificial neural network (ANN) of a backpropagation algorithm. The ANN uses the
288 cosine transformed time-of-the-day and day-of-the-year, air temperature, relative humidity, wind speed and
289 direction, atmospheric pressure, precipitation, downward shortwave radiation, cloud cover, soil temperature, and
290 EVI.

291 Flux partitioning into photosynthesis and ecosystem respiration from the EC measured F_C requires additional
292 information and data processing (e.g., Stoy et al., 2006). It is important to partition theStochastic F_C partitioning
293 methods were recently applied by reprocessing EC observation data with auxiliary data and provided useful
294 knowledge on carbon cycle (Hiller et al., 2011; Crawford and Christen, 2015; Menzer and McFadden, 2017;
295 Stagakis et al., 2019). Here we partition the measured F_C into four contributing components (i.e., RE , GPP , E_R ,
296 and E_B in Eq. 2) to investigate their biotic and abiotic controlling factors in an artificially constructed park. This
297 study applies for a statistical partitioning method described in Lee et al. (2021).Menzer and McFadden (2017)
298 estimates anthropogenic emissions with traffic volume and air temperature in winter with wind directions when
299 anthropogenic emission is dominant in net CO_2 fluxes. This study extends the statistical partitioning method by
300 Menzer and McFadden (2017). Similar to Menzer and McFadden (2017), our partitioning method chooses
301 temporal subsets so that some components in Eqn. (2) are insignificant with footprint weighted road fraction so
302 that the statistical partitioning is applicable even when E_R is not negligible. In this way, RE is estimated as a
303 function of temperature first and GPP is finally estimated after modelling E_R and E_B based on the traffic volume
304 and high-resolution footprint weighted road fraction (see Fig. 1a and Table 1 in Lee et al. (2021)). Our estimations
305 on anthropogenic emission from vehicle and building show good correlation with inventory data such as visitor
306 counts, traffic volume, and natural gas consumption in the park. More information and relevant figures on the flux
307 partitioning are available in Lee et al. (2021).

308 **3 Results and discussion**

309 **3.1 Surface energy ~~balance~~fluxes**

310 ~~The SEB~~Surface energy fluxes at the SFP shows typical seasonal variations over natural forest canopies with the
311 seasonal march of the East Asian monsoon (Fig. 4) (Hong and Kim, 2011; Hong et al., 2019b; Hong et al., 2020).
312 ~~In summer, there~~There are lengthy rainy spells and large temporal variabilities of meteorological conditions ~~with~~
313 ~~the impacts of~~during the East Asian summer monsoon period (Fig. ~~2d~~1d). This heavy rainfall causes substantial
314 decreases in K_L , and thus Q^* , with large temporal variations, thereby leading to the mid-summer depression of
315 surface fluxes (Fig. ~~2e~~1c and 4). Q^* also reaches its maximum in spring rather than in summer and decreases

316 gradually from spring to winter (Fig. 4). ~~More~~The annual ration of Q_E to Q^* at the SFP is smaller than its global
317 average of 0.55 and values over forest canopies at similar latitudes in the East Asia (Falge et al., 2001; Suyker
318 and Verma, 2008; Khatun et al., 2011). ~~half~~In summer, about 50% of Q^* is partitioned to Q_E , and Q_H is minimum
319 in summer owing to~~because of~~ the ample water supply from the summer rainfall. ~~However,~~ Q_H is maximum in
320 spring and even larger in winter, despite the relatively smaller Q^* , because of the cold and dry climatic conditions
321 induced by the winter monsoon. Accordingly, the seasonal mean Bowen ratio ($\beta = \sum Q_H / \sum Q_E$) ranges from near
322 zero (summer) to approximately 4 (winter) with its daily maximum around 9 in early January 2015 (Fig. 5).
323 ~~Notably,~~ β in the SFP is consistently lower than the high-rise, high-density residential area (i.e., the EP site)
324 because of the ET from the vegetative canopies and the unpaved surfaces in the urban forest. ~~This difference~~
325 ~~between the two distinct sites confirms that urban forests are responsible for substantial changes in the thermal~~
326 ~~environment in terms of Q_H and Q_E , as well as their related air and surface temperatures because of more~~
327 ~~evaporative cooling in green spaces compared to impervious surfaces such as roads and buildings in urban areas~~
328 ~~(Oke et al., 2017)~~ Daytime Bowen ratio in summer is about 0.6, which is smaller in other urban sites but is similar
329 to suburban sites of the similar vegetation cover mainly because of the small fraction of impervious spaces around
330 the SFP station (Table 2).

331 ~~The SEB~~ Surface energy fluxes also shows ~~interannual~~ annual variabilities over ~~forest canopies~~ influenced by the
332 timing of the onset and duration of the summer monsoon, similarly to natural forest in East Asia, (Hong and Kim,
333 2011) (Fig. ~~6~~ 1, 4, and 5). As discussed in Section 2.2.1-2, annual precipitation is much larger in the first year than
334 in the second year because of the interannual variations in the East Asian summer monsoon activity, thereby
335 making substantial differences in surface radiative fluxes. Furthermore, Q_E shows the difference between the first
336 and second years of the observation, particularly by responding to such interannual variability of radiation. In the
337 first year ~~of the observation,~~ Q_E is more than 300 W m^{-2} and has a relatively larger temporal variability because
338 of the frequent rainfall events in summer, compared to the second year. However, it is notable that interannual
339 variability of surface fluxes are relatively weaker than natural forest in this region which will be better manifested
340 in ET and its ratio to precipitation.

341 Evapotranspiration rate, which is equivalent to Q_E , ranges from 5 mm month^{-1} in January 2015 to 74 mm month^{-1}
342 in August 2013, and the annual ET values are 367 and 320 mm year^{-1} in the first and second years, respectively
343 (Fig. 1 and 5 and Table-~~2~~ 3). The ET values correspond to 29.3% and 34.3% of the annual precipitations and 49 %
344 and 42% of net radiation, respectively. The annual ET in the second year is smaller than that in the first year with
345 extensive drought in the second year. (Fig. ~~2d~~ 2d). The difference in ET between the two consecutive years (i.e., 48
346 mm) mainly occurred in summer (42 mm), especially in August (30 mm). ~~It has been reported that approximately~~
347 ~~55% of the net radiation is partitioned to latent heat flux in forest canopies globally (Falge et al., 2001; Suyker~~
348 ~~and Verma, 2008). The annual ET to net radiation from the urban forest is smaller than this global average and it~~
349 ~~is also smaller than that of forests at similar latitudes in the East Asia (Khatun et al., 2011).~~ ~~The annual~~
350 ~~ET in the second year is smaller than that in the first year with extensive drought in the second year.~~ However, it
351 is notable that the ET in the second year shows only an approximately 12% decrease ~~compared to the first year,~~
352 despite a substantial decrease in precipitation (26% decrease) and the similar net radiation in the second year,

353 compared to the first year (Table 23). Although the summer monsoon provides ample water to the ecosystem, its
354 delay and weakness result in severe drought and stress to the ecosystem in this region (Hong and Kim, 2011);
355 however, such ecosystem stress, such as the shrinking of ET and carbon uptake, is inexplicitly has not been
356 extensively investigated for the urban forest. We speculate that artificial irrigation by a sprinkler mitigated
357 ecosystem stress to a certain degree in the urban forest.

358 3.2 Air temperature

359 Figure 6 shows the mean diurnal pattern of the air temperature difference between the AVG and SD near the SFP
360 ($\Delta T_{air} = T_{air_AVG} - T_{air_SD}$ hereafter) before and after the park construction in summer. Notably, ~~ΔT_{air} is always~~
361 ~~positive during the entire summer season (i.e., AVG is warmer than SD) and shows distinct impacts in terms of~~
362 ~~magnitude and diurnal variations after the park construction. The warming trend is evident at the AVG ($p < 0.015$),~~
363 ~~wherein there were no changes in the urban structure and function around them. The warming rate at the AVG is~~
364 ~~$3.0\text{ }^{\circ}\text{C century}^{-1}$, which corresponds to the warming rate reported in the high-rise urban area in Seoul (Hong et al.,~~
365 ~~2019a). However, the warming rate around the SFP is approximately $1.6\text{ }^{\circ}\text{C century}^{-1}$, which is smaller than that~~
366 ~~of the AVG and other urban areas in Seoul and is comparable to the global mean warming rate of $0.9\text{ }^{\circ}\text{C century}^{-1}$~~
367 ~~(Hansen et al., 2010; Hong et al., 2019a).~~

368 Notably, such a lower warming trend around the SFP mainly occurs in the afternoon when ET is dominant. This
369 difference will be larger if we consider that the measurement height at the AVG is higher than that at the SD
370 (Table. 1). The maximum ΔT_{air} is approximately $0.3\text{ }^{\circ}\text{C}$ around 10:00 before the park construction (Fig. 6a) and
371 increases up to approximately $0.5\text{ }^{\circ}\text{C}$ with its peak occurrence shifting from the morning to the afternoon (i.e.,
372 around 14:00) after the construction (Fig. 6b). This peak time in the afternoon is coincident with the time when
373 photosynthesis is the highest in the vegetation; thus, Q_E increases in summer. Our results indicate that the thermal
374 mitigation of the urban forest is important as a result of increases in ET, especially if we consider that the SFP
375 area was originally planned to be developed as a high population multipurpose building complex.

376 3.3 Urban heat island intensity

377 The influence of urban forests on summer temperature produces also evident traces in UHIi. Figure 7 shows the
378 mean diurnal variation of UHIi at the SFP and AVG during summer. Apparently, the UHIi of the SFP (UHIi^S
379 hereafter) and ~~AVG (UHIi^A CBD (UHIi^C hereafter)~~ gradually increases after mid-afternoon and is the largest at
380 night. (Fig. 6). This diurnal pattern is consistent with previous reports in cities exposed to different geographical
381 and climatic conditions because rural areas cool faster than urban areas (Oke et al., 2017). Additionally,
382 ~~UHIi^A UHIi^C~~ is positive throughout all days ranging from 0.2 – $2.2\text{ }^{\circ}\text{C}$ (i.e., warmer than rural area, GP) and is
383 greater than UHIi^S by 0 – $1.5\text{ }^{\circ}\text{C}$. ~~A possible~~The reason for this stronger ~~UHIi^A UHIi^C~~ is that the ~~AVG CBD~~ stations
384 are ~~located~~ in the central business district; thus, the densities of buildings surrounding these stations are much
385 higher than those surrounding the SFP station. At night (19:00–06:00), ~~UHIi^A UHIi^C~~ and UHIi^S are approximately
386 $1.8\text{ }^{\circ}\text{C}$ and $1.4\text{ }^{\circ}\text{C}$, respectively. The maximum UHIi difference between the ~~AVG CBD~~ and SFP was $0.7\text{ }^{\circ}\text{C}$ in
387 2013 and $0.5\text{ }^{\circ}\text{C}$ in 2014.

388 Around sunrise, sharp declines in the UHI are observed because the air temperature near the urban area increases
389 relatively slowly as urban fabrics, such as asphalt, brick, and concrete, have larger heat capacities and less sky
390 view factors than the rural areas (Oke et al., 2017). Eventually, this slow increase in the air temperature reduces
391 the differences in T_{air} among the stations, thereby reducing the UHI. The minimum $\text{UHI}^A - \text{UHI}^C$ values were
392 0.3 °C (2013) at 09:30 and 0.2 °C (2014) at 08:30, while the minimum UHI^S occurs at 10:30 with values of –
393 0.1 °C (2013) and 0.0 °C (2014). This implies that the timing of the minimum UHI is delayed in the SFP compared
394 to the AVG. ~~Our findings indicate that the urban forest has a similar air temperature in the daytime as compared
395 to the rural area (i.e., GP) where has a lower thermal admittance because of its location within the airport.
396 Especially when there is strong ETCBD. Notably, when there is strong ET (i.e., the first year) and more time is
397 required to warm the SFP surface, the urban-rural difference in thermal admittance becomes relatively small. This
398 can be attributed to the higher thermal capacity of the wetter soil of the SFP as a result because of artificial
399 irrigation and the absence of impervious surfaces (Oke et al., 1991).~~

400 The diurnal variations in UHI^S also show the interannual variability in both amplitude and steepness over the two
401 consecutive years. Despite the similar summertime $\text{UHI}^A - \text{UHI}^C$ for both years, the daytime UHI^S in 2013 was
402 approximately 0.2 °C lower than that in 2014. Notably, the summer Q_E was greater in 2013 than in 2014, and this
403 observed summertime asymmetric difference between the SFP and AVGCBD stations was not found in the winter
404 when ET was negligible (not shown here).

405 ΔT_{air} is always positive during the entire summer season (i.e., CBD is warmer than SD) and shows distinct impacts
406 on magnitude and diurnal variability after the park construction (Fig. 7). This difference will be larger if we
407 consider that the measurement height at the CBD is higher than that at the SD (Table. 1). Notably, this temperature
408 contrast mainly occurs in the afternoon when ET is dominant. The maximum ΔT_{air} is approximately 0.3 °C around
409 10:00 before the park construction (Fig. ~~Our results suggest that urban forests can play a significant role in~~
410 mitigating the thermal environment7a) and increases up to approximately 0.5 °C with its peak occurrence shifting
411 from the morning to the afternoon (i.e., around 14:00) after the construction (Fig. 7b). This peak time in the
412 afternoon is coincident with the time when photosynthesis and Q_E are highest. The annual mean of the maximum
413 UHI in the SD is about 4 °C and does not change significantly after the park construction compared to the CBD
414 regions (Hong et al., 2019a). On the contrary, the daytime maximum UHI of the SD in summer decreases after
415 the park construction (not shown here). Our results indicate that the thermal mitigation of the urban forest is
416 important because of the wetter soil surface of the park and subsequent increases in Q_E , compared to the
417 impervious surfaces in urban areas. ~~In particular, our findings indicate~~ This is especially true if we consider that
418 the SFP area was originally planned to be developed as a high-population multi-purpose building complex. Our
419 findings emphasize that the heat mitigation of the urban forest depends on the ratio of Q_E to net radiation. Indeed,
420 there is an evident negative relationship between daytime Q_E and air temperature differences between the SFP and
421 AVGCBD stations (Fig. 8). As K_d is more partitioned to Q_E , T_{air} of the SFP decreases more than that of the
422 AVGCBD, and the maximum temperature difference is observed in the summer season. The SFP is cooler than
423 the AVGCBD by up to 0.6 °C, but the SFP is warmer than the AVGCBD during the winter-dormant season when
424 ET is small. Our findings confirm that urban forests are responsible for substantial changes in the thermal

environment in terms of O_H and O_E , as well as their related air and surface temperatures because of more evaporative cooling in green spaces compared to impervious surfaces such as roads and buildings in urban areas (Oke et al., 2017).

3.4.3 Temporal dynamics of net CO₂ exchange

Figure 9 shows the diurnal evolution of F_C and footprint weighted road fraction (λ). Overall, the mean daytime F_C is negative (i.e., carbon uptake) in the summer (June–August), indicating that photosynthesis, the only carbon sink, is dominant in the growing season (Fig. 9). This carbon uptake period is coincident with the active vegetation manifested by increases in EVI (not shown here). Summertime photosynthetic carbon uptake (GPP) has a daily average of $7.6 \mu\text{mol m}^{-2} \text{s}^{-1}$ with a maximum of $18.9 \mu\text{mol m}^{-2} \text{s}^{-1}$ around 12:30 (Fig. 8a in Lee et al., 2021) and 10). A daily minimum F_C also occurs around 12:30 with the maximum photosynthetic carbon uptake during this time accordingly. The vegetation around the SFP absorbs more CO₂ than carbon sources and F_C becomes negative only during the summer daytime. However, because of substantial amounts of anthropogenic emissions and ecosystem respiration, F_C changes from negative (i.e., carbon sink) to positive values (i.e., carbon source) even around 16:30 in summer unlike in natural ecosystems, despite the substantial downward shortwave.

CO₂ uptake is highest in June, with a maximum of approximately $13 \mu\text{mol m}^{-2} \text{s}^{-1}$ (Fig. 9a). In the middle of summer (4th and 31st two-week data in Fig. 9a), CO₂ uptake decreases significantly because photosynthesis is limited because of the reduced K_d by cloud and rainfall with the onset of the summer monsoon (Fig. 2e1c). This mid-summer depression of carbon uptake has been reported in the Asian natural vegetations (e.g., Kwon et al., 2009; Hong and Kim, 2011; Hong et al., 2014). Higher/Greater reduction in CO₂ uptake observed in 2013 than in 2014 was attributed to a longer monsoon period in 2013. Indeed, from 8 to 21 July 2013 (4th two-week data in Fig. 9a), the accumulated precipitation was approximately 400 mm for two weeks, and the daily averaged K_d was only 70 W m^{-2} .

The vegetation around the SFP absorbs more CO₂ than is emitted by local carbon sources and F_C is negative only during the summer daytime. Because of substantial amounts of anthropogenic emissions and ecosystem respiration, F_C changes from negative (i.e., carbon sink) to positive values (i.e., carbon source) even around 16:30 in summer unlike in natural ecosystems, despite the substantial downward shortwave. As photosynthesis decreases, F_C changes (e.g., Desai et al., 2008; Hong et al., 2009; Alekseychik et al., 2017; Chatterjee et al., 2020). As photosynthesis decreases, F_C changes to positive values from November. During the non-growing season (i.e., late autumn, winter, and early spring), anthropogenic emissions were also dominant because photosynthesis and ecosystem respiration decrease with smaller K_d and lower temperatures. During these periods, F_C had minimum values at 04:00–05:00 and increases until 15:00–16:00. Therefore, the diurnal variations in F_C mainly followed the traffic volume (Fig. 4a in Lee et al., 2021), and there is also a clear positive relationship between F_C and λ (23rd, 45th, and 47th two-week data in Fig. 9 Fig. 4 in Lee et al., 2021). It is also noteworthy that the peak

459 time of F_C (16:00) is earlier than the peak time of λ (18:00) from December to early March because E_B is the
460 largest at around 15:00–16:00, indicating that E_R and E_B are the controlling factor of F_C in this period.

461 ~~With such apparent~~The seasonal F_C variation, ~~it is notable that its variability also~~ depends on the spatio-temporal
462 distribution of CO₂ sources and flux ~~source-area footprint~~ because the latter covers various land use with changes
463 in wind direction and atmospheric stability (Fig. 10). In autumn, the main wind direction ~~changed~~changes to the
464 north as the synoptic conditions change ~~particularly as discussed in section 2~~ (Fig. 32); therefore, λ is smaller in
465 autumn compared to other seasons (Fig. 9b). For example, the road fraction ~~was~~is smallest at < 1% from midnight
466 to midday and < 3% during the afternoon in October and November (11th, 12th, 36th, and 37th two-week data in
467 Fig. 9b). In these periods, the nighttime F_C ~~showed~~shows the lowest value of approximately $2.9 \mu\text{mol m}^{-2} \text{s}^{-1}$,
468 which ~~was~~is attributable to the smallest road fraction, lower respiration, and minimal heating usage.

469 In early spring, λ ~~was~~is generally larger; thus, E_R ~~played~~plays a significant role in F_C , and E_B ~~also remained~~remains
470 non-zero until early April ~~because of anthropogenic emission by hot water and space heating in the building within~~
471 ~~the footprint~~, thereby resulting in the largest F_C in this period. With a shutdown of the heating system (i.e., zero
472 E_B) and the sprouting of leaves in April, there ~~was~~is a sharp decrease in F_C (Fig. 10b and 10c). From December
473 to March, CO₂ emissions ~~increased~~increase up to $30 \mu\text{mol m}^{-2} \text{s}^{-1}$ with larger variability ~~in the south-west direction~~
474 because of intermittent anthropogenic emissions from the park facility ~~building in the south-west directions~~ (due
475 to space heating and boiling water), as well as the relatively increased contribution of vehicles on the road in the
476 western part of the site- (Fig. 10b).

477 Although the positive F_C in the winter ~~decreased~~decreases in spring, its magnitude ~~showed~~shows directional
478 differences (Fig. 10c). On the eastern side, the mean F_C ~~showed~~shows a negative value in May, whereas it
479 ~~remained~~remains positive on the western side (210–270°) until May. ~~Therefore, these~~These findings further
480 ~~indicating~~indicate the different contributions of various carbon sources and sinks among the different wind
481 directions. For the wind directions from the north to the east (0–120°), F_C ~~showed~~shows a relatively weaker carbon
482 sink than other directions because of the relatively low tree fraction in this direction (Fig. 10a and 10c). On the
483 southern side (150–180°) having the highest tree cover fraction, a maximum carbon uptake ~~is~~ about $15 \mu\text{mol m}^{-2}$
484 ~~s⁻¹ on average was found~~ in June. However, despite the dense vegetation on the south and west side (120–330°),
485 the F_C magnitude was much smaller than that of other natural forests. This is related to the anthropogenic
486 emissions from vehicles on the roads which is discussed in section 3.65.

487 3.54 Light use efficiency of biogenic CO₂ components

488 F_C at the SFP shows a typical light response to the photosynthetically active radiation (PAR) in a way similar to
489 natural ecosystems in spite of anthropogenic CO₂ sources from vehicles (Fig. 11a and 11b11). However, this light
490 response in the urban forest is a distinct contrast ~~with the non-dependent to~~ F_C in high-rise high-population
491 residential areas in Seoul under the same climatic conditions ~~(that does not respond to PAR (i.e., EP station)).~~
492 Importantly, GPP , NBE , and F_C show different trends on PAR depending on the direction. As stated in Section
493 2.1+2.2 and 3.43, the western side has a higher density of trees as against more grass on the eastern side, and

494 biotic CO₂ uptake from the western side is substantially larger than that on the eastern side. Accordingly, the slope
 495 of the light response curve for PAR on the western side is steeper than on the eastern side. F_C at zero PAR (F_{C_0})
 496 is larger on the western side (9.7 $\mu\text{mol m}^{-2} \text{s}^{-1}$) than on the eastern side (5.1 $\mu\text{mol m}^{-2} \text{s}^{-1}$) because of a contribution
 497 of E_R from roads on the western side of the tower.

498 NBE shows a comparable light response to natural vegetation (e.g., Schmid et al., 2003). A rectangular hyperbolic
 499 equation has been used to examine the light response of NBE and elucidate the directional differences in carbon
 500 uptake:

$$501 \quad NBE = -GPP + RE = -\frac{\alpha \cdot GPP_{sat} \cdot PAR}{GPP_{sat} + \alpha \cdot PAR} + RE \quad (3)$$

502 ~~where α is the quantum yield efficiency (the initial slope of the light response curve), GPP_{sat} is the potential rate~~
 503 ~~of the ecosystem CO₂ uptake.~~ α is approximately 0.0651 and 0.0558 $\mu\text{mol CO}_2 (\mu\text{mol photon})^{-1}$ on the western
 504 and eastern sides, respectively. Notably, α on the western side is comparable to the high initial quantum yield in
 505 crops and subtropical forests in East Asia (Hong et al., 2019b; Emmel et al., 2020). Additionally, GPP_{sat} is 30.9
 506 and 12.7 $\mu\text{mol m}^{-2} \text{s}^{-1}$ on the western and eastern sides, respectively. In addition, the light saturation points are at
 507 a PAR of 1500 $\mu\text{mol m}^{-2} \text{s}^{-1}$ on the eastern side, which occur at a relatively lower PAR than on the western side.
 508 Daytime respiration ~~estimated~~estimates from equation (3) is 6.7 and 6.3 $\mu\text{mol m}^{-2} \text{s}^{-1}$ on the western and eastern
 509 sides, respectively. Because GPP is related to PAR, the difference in monthly cumulative GPP between the two
 510 years shows a close relationship with the difference in the monthly sunshine duration ($r^2 = 0.75$, not shown here),
 511 ~~thereby~~ suggesting a possible impact of change in the onset of the summer monsoon on urban forests.

512 The magnitude of NBE from the western side is larger than that from ~~the~~ suburban area ~~having~~with about 50%
 513 vegetative fraction in Montreal, Canada (Fig. 7b in Bergeron and Strachan, 2011) and F_C from a highly vegetated
 514 environment of about 67% vegetative fraction in Baltimore, USA (Crawford et al., 2011). Also, GPP from the
 515 western side is comparable to the dense forest canopies in subtropical forests in Korea (Hong et al., 2019b),
 516 deciduous forest ecosystems (Goulden et al., 1996), and a mixed hardwood forest ecosystem (Schmid et al., 2000).
 517 However, NBE from the eastern side is similar to F_C from the suburban areas of about 44%, 50%, and 64%
 518 vegetative fraction in Swindon, UK (Ward et al., 2013) and Montreal, Canada (Bergeron and Strachan, 2011), and
 519 Ochang, Korea in the same climate zone (Hong et al., 2019b), respectively.

520 **3.65 Annual budget of CO₂ sources and sink**

521 ~~The annual budget of the F_C and its components is summarized in Table 3.~~ The annual sums of the GPP and RE
 522 in the SFP are 4.6 kg CO₂ m⁻² year⁻¹ (1244 gC m⁻² year⁻¹) and 5.1 kg CO₂ m⁻² year⁻¹ (1378 gC m⁻² year⁻¹),
 523 respectively. ~~(Table 4).~~ This photosynthetic carbon uptake is smaller than its global mean GPP in natural
 524 deciduous broadleaf forests with similar annual precipitation and annual mean air temperature (total 8 years of
 525 data from 4 sites of FLUXNET2015 dataset reported in Pastorello et al., 2020) and similar to that of deciduous
 526 broadleaf forests in East Asia (Awal et al., 2010; Kwon et al., 2010) (Table 4). ~~Our speculation is, however,~~5).
 527 However, we note that this GPP is relatively larger if we consider the low vegetation fraction and leaf area index

528 (LAI) at our urban park. ~~Indeed, GPP is comparable to values reported in other urban sites if it is scaled with the~~
529 ~~vegetation cover fraction.~~ Previous studies have shown that the GPP of urban vegetation is scaled with vegetation
530 cover fraction with an increase of about 0.7 kg CO₂ m⁻² year⁻¹ per 10% increase in vegetation cover fraction (Awal
531 et al., 2010; Crawford and Christen, 2015; Velasco et al., 2016; Menzer and McFadden, 2017). Indeed, GPP at
532 the SFP with a 46.6% vegetation cover fraction is approximately 1.5 kg CO₂ m⁻² year⁻¹ which is larger than this
533 scale values reported in other urban sites if it is scaled with the vegetation cover fraction (Fig. 12a).

534 ~~Eventually, Despite this large larger GPP results in a resulting smaller F_C eventually, there is no~~ substantial decrease
535 in F_C when they are scaled by vegetation fraction, ~~suggesting large contribution of RE (Fig. 12b).~~ ~~Hong et al.~~
536 ~~(2019b) reported There was~~ a linear decrease in F_C of approximately 3.0 kg CO₂ m⁻² year⁻¹ per 10% increase in
537 vegetation cover fraction based on the observed F_C across an urbanization gradient ~~in Korea (Fig. (Hong et al.,~~
538 ~~2019b and references therein).~~ ~~12b).~~ The annual F_C in the SFP ~~of 7.1 kg CO₂ m⁻² is 1.2 kg CO₂ m⁻² year⁻¹ smaller~~
539 ~~than not so much different from other similar cities and~~ this scaled relationship ~~(i.e., more carbon uptake).~~ ~~In~~
540 ~~particular, F_C in the SFP is approximately 3.0 kg CO₂ m⁻² year⁻¹ less than that in recently developed high-rise high-~~
541 ~~population urban areas in Seoul. Our results suggest that efficient management of urban forests, such as regular~~
542 ~~irrigation and fertilization, can be an efficient way to adapt and mitigate climate change by increasing CO₂ uptake~~
543 ~~in artificial forest constructions in East Asia.~~

544 Meanwhile, RE at our site is much larger than that in natural temperate deciduous forests in East Asia the similar
545 climate zone (Takanashi et al., 2005; Kwon et al., 2010) and similar to that in the urban forest in East Asia (Awal
546 et al., 2010), as well as to the global mean RE over forests with similar annual precipitation and annual mean air
547 temperatures (Pastorello et al., 2020). Put differently, the urban forest considered in our study is an outlier
548 compared to other natural forest canopies and urban forests because RE/GPP > 1 (Table 45). Autotrophic
549 respiration is considered to be approximately half of GPP as a rule of thumb (Piao et al., 2010), which corresponds
550 to approximately 45% of the RE at our site, thereby indicating a large contribution of heterotrophic respiration to
551 RE. Indeed, it was reported that soil respiration at the same site was approximately 4 kg CO₂ m⁻² year⁻¹ (Bae and
552 Ryu, 2017). The reason for the large soil organic carbon was mainly because rice cultivation was carried out in
553 this region before the 1950s, and organic carbon-rich soil was transplanted during the SFP construction, and
554 fertilizers were applied regularly. It has also been reported that RE is enhanced in urban areas because of the
555 relatively warmer temperature in urban regions (i.e., UHI) (Awal et al., 2010). Notably, Q₁₀ (the rate by which
556 respiration is multiplied when temperature increases by 10 °C) is about 1.9 at the site and matches the Q₁₀ value
557 for ecosystem respiration (2.2 ± 0.7) calculated for natural forests across 42 FLUXNET sites (Mahecha et al.,
558 2010). Further analysis based on the observed Q₁₀ and the UHI at the SFP indicates that UHI leads to an
559 approximately 5% increase in RE.

560 ~~Figure 13 shows the monthly cumulative sum of the F_C and its partitioned components.~~ Seasonal variations in the
561 strength of carbon sources and sink as well as F_C are mainly regulated by the biogenic component in summer and
562 the anthropogenic component in winter. ~~(Fig. 13).~~ Furthermore, F_C is minimum in June, despite the similar GPP
563 from June to August because of the relatively smaller RE during the summer season. Even in summer,
564 photosynthetic carbon uptake is balanced with ecosystem respiration and does not offset all biotic and

565 anthropogenic emissions, thus resulting in positive F_C values throughout the year. In winter, E_B is dominant with
566 negligible GPP and RE due to cold temperatures, and E_R also becomes larger than RE from November. E_R shows
567 apparent seasonal variation in wind direction and atmospheric stability. Its magnitude is about $0.0666 \mu\text{mol m}^{-2}$
568 $\text{veh}^{-1} \text{h s}^{-1}$ in neutral condition and consistent with the value in the inventory data (Lee et al., 2021). The average
569 monthly traffic speed for the road in front of the SFP is $50\text{--}60 \text{ km h}^{-1}$ (based on the January 2014 data from the
570 Seoul Metropolitan Government Traffic Speed Report), and the CO_2 emission rate is approximately 150 g CO_2
571 $\text{km}^{-1} \text{veh}^{-1}$ based on the emission data at this speed (Kim et al., 2011). With the width of the ten-lane road (25--
572 30 m), the inventory-based slope (i.e., CO_2 emission rate per vehicle per area per half-hour) is approximately in
573 the range of $0.0631\text{--}0.0757 \mu\text{mol m}^{-2} \text{veh}^{-1} \text{half-hour s}^{-1}$ ($\cong 150 \text{ gCO}_2 \text{ km}^{-1} \text{veh}^{-1} \times 1/30$ or $1/25 \text{ m}^{-1} \times 1/44 \text{ mol}$
574 $\text{gCO}_2^{-1} \times 10^{-3} \text{ km m}^{-1} \times 10^6 \mu\text{mol mol}^{-1} \times 1/1800 \text{ half-hour s}^{-1}$).

575 There is an evident yearly difference in individual carbon sources and sink in two consecutive years. E_B is mainly
576 caused by heating buildings and hot water in park facilities using natural gas. Notably, E_B is highly correlated with
577 gas consumption in SFP during winter on monthly basis ($R^2 = 0.94$; Fig. 6 in Lee et al., 2021). ~~Notably, E_B is~~
578 ~~also E_B is~~ smaller in the first year because of the relatively smaller number of park visitors and consequently
579 smaller gas consumption, compared to the second year. ~~Indeed, E_B is highly correlated with gas consumption in~~
580 ~~SFP during winter on a monthly basis ($R^2 = 0.94$; Fig. 6 in Lee et al., 2021).~~ Eventually, these annual differences
581 lead to a smaller annual mean total F_C in the first year than in the second year (Table 3). ~~However,~~ RE is
582 maximum in the August of the first year, while it is highest in July ~~of~~ in the second year because the monthly mean
583 air temperature is highest in August of the first and July of the interannual second year with annual variations in
584 air temperature with changes in the timing and duration of the East Asian summer monsoon, of which impacts
585 have also been reported in natural vegetation in the same region (Hong and Kim, 2011; Hong et al., 2019b). ~~In~~
586 ~~other words, the monthly mean air temperature is highest in August of the first and July of the second year because~~
587 ~~of the short East Asian monsoon period and drought in July of the second year. However, the~~ 2019b). GPP in
588 summer is relatively smaller in the first year by the mid-summer depression of solar radiation because of the
589 elongated monsoon period ~~(but annual sums of GPP are similar in two years (Table 4 and Fig. 2). However,~~ 13).
590 GPP does not shrink in the second year of significant drought because ~~there is~~ of ample water supply by a sprinkler.
591 Eventually, F_C in the SFP is approximately $3.0 \text{ kg CO}_2 \text{ m}^{-2} \text{ year}^{-1}$ less than that in recently developed high-rise
592 high-population urban areas in Seoul. Our results ~~emphasize the important role of forest suggest that efficient~~
593 ~~management in enhancing carbon of urban forests, such as regular irrigation and fertilization, can be an efficient~~
594 ~~way to adapt and mitigate climate change by increasing CO_2 uptake and evaporative cooling despite the low~~
595 ~~vegetation fraction in artificial forest constructions in East Asia.~~

596 4 Summary and conclusions

597 This study reported two-year surface fluxes of energy and CO_2 measured by the eddy covariance method ~~while~~
598 ~~also examining in order to examine~~ the role of artificially generated urban forests in mitigating air temperature and
599 anthropogenic CO_2 emissions. The study area is ~~located in the East Asian monsoon region, characterized by a~~
600 ~~lengthy summer rainy season. During the measurement period, the second year was contrasted with the first year~~

601 ~~because of the drought compared to the normal climate condition in the first year. The study region is an urban~~
602 ~~park with an artificially planted forest in the Seoul Metropolitan Area. The urban forest had a heavy traffic volume~~
603 ~~around it and was~~ redeveloped from a racetrack and factory in the mid-2000s. ~~where is influenced by a lengthy~~
604 ~~summer rainy season during the East Asian summer monsoon.~~ To examine the mitigation of air temperature, this
605 study ~~compared~~compares meteorological conditions in the urban forest with the surrounding high-rise high-
606 population urban areas. This study ~~also proposed~~applies for the ANN-based gap filling and a statistical CO₂ flux
607 partitioning method based on temporal subsets of flux data and high-resolution footprint-weighted land use data
608 to understand the abiotic and biotic contributions to F_C .

609 Surface energy ~~balance~~fluxes in the SFP is influenced by the summer monsoon, and more energy is distributed to
610 Q_E than Q_H in the summer ~~when vegetation is active, similar in the growing season, similarly~~ to natural forests in
611 this climate zone. ~~Therefore, the~~The Bowen ratio in this urban forest ranges from near 0 (summer) to about 4
612 (winter), which is lower throughout the year than that of high-rise and high-density residential areas in Seoul. This
613 suggests that the vegetation and unpaved surfaces of urban forests facilitate more evaporative cooling compared
614 to the impervious surfaces in urban areas. ~~Furthermore, ET decreased in~~During the measurement period, the
615 second year ~~when there was a~~is contrasted with the first year because of the drought compared to the normal
616 ~~climate condition in the first year.~~ Notably, ET decreases in the second year, but this drop ~~was~~is not as much as
617 the reduced precipitation ~~if we consider the substantial and its related~~ changes in ~~precipitation and~~radiative forcing
618 ~~in two consecutive years~~during the drought because of the artificial irrigation by a sprinkler mitigated ecosystem.

619 It is also evident that the urban forest reduced the warming trend and UHI around the study area. Air temperature
620 in the SFP ~~was~~is lower than the surrounding area, but this coolness ~~was~~is reinforced after the park was created.
621 The warming trend ~~diminished~~diminishes after the construction of the park and ~~was~~is smaller than that in other
622 urban regions in the Seoul Metropolitan Area. In addition, the construction of the park ~~delayed~~delays the timing
623 of the maximum temperature difference between the urban forest and high-rise commercial from the morning to
624 the afternoon, coinciding with the timing of the maximum Q_E . The SFP shows a ~~general~~typical diurnal UHI
625 variation pattern, which has a higher temperature at night than in rural areas. However, the UHI in SFP is lower
626 by 0.6 °C in summer compared to the surrounding urban area, and the ~~time of the~~ minimum peak time is delayed,
627 possibly because vegetation and permeable soils in SFP have a larger thermal capacity. Notably, UHI
628 ~~decreased~~decreases more in the partitioning of incoming energy into latent heat fluxes. ~~As a rule of thumb, and~~
629 there was cooling by 0.2 °C compared to the surrounding urban area if Q_E/K_d increased by 10%.% ~~in this study.~~

630 Net CO₂ exchange at the urban forest ~~showed~~shows typical temporal variations in natural forest canopies
631 influenced by the East Asian summer monsoon ~~(Hong and Kim, 2011; Hong et al., 2019b).~~. A mid-summer
632 depression of carbon uptake ~~was~~is observed with the onset of the summer monsoon, like vegetation in the East
633 Asian monsoon region. The GPP ~~was~~is estimated by the statistical partitioning method, and the non-zero GPP
634 period ~~was~~is coincident with the active vegetation of the significant vegetation index. Summertime photosynthetic
635 carbon uptake ~~had~~has a daily average of 7.6 $\mu\text{mol m}^{-2} \text{s}^{-1}$ with a maximum of 18.9 $\mu\text{mol m}^{-2} \text{s}^{-1}$ around 12:30.
636 However, even during the growing season, vegetative carbon uptake ~~was~~is insufficient to offset anthropogenic
637 CO₂ emissions and ecosystem respiration on a time scale of > 1 day. Our estimations of anthropogenic CO₂

638 emissions from vehicles and buildings ~~agreed~~agree with the estimations based on inventory data such as CO₂
639 emission rate of vehicles and monthly gas consumption, and their annual budgets each ~~had~~have a comparable
640 magnitude to *GPP*.

641 Annual *GPP* of the urban forest ~~was~~is relatively smaller than that of the forest in East Asia exposed to similar
642 climatic conditions because of the relatively smaller vegetation cover fraction and LAI. However, it ~~was~~is larger
643 than the *GPP* expected from the relationship from previous urban studies if it ~~was~~is normalized by the vegetation
644 cover fraction. *RE* is, however, much larger than that in the temperate East Asian forests and ~~is~~ similar to the
645 urban forest in East Asia. We speculate that soil respiration ~~enhanced~~enhances such large ~~ecosystem respiration~~*RE*
646 by relatively warmer temperatures in a city and rich soil organic carbon in the SFP. ~~Eventually, the~~The annual
647 mean total *F_C* is 7.1 kg CO₂ m⁻² year⁻¹, which is smaller than the estimate from the scaling between annual total
648 *F_C* and vegetation fraction (Hong et al., 2019b). Because of the spatial heterogeneity, *F_C* and its components
649 showed directional changes. *NBE* from the eastern side is similar to ~~*F_C* of that in~~ suburban areas with
650 approximately 44%, 50%, and 64% vegetative fraction in Swindon, UK (Ward et al., 2013) and Montreal, Canada
651 (Bergeron and Strachan, 2011), and Ochang, Korea in the same climate zone (Hong et al., 2019b), respectively.
652 However, the *NBE* and *GPP* from the western side are comparable to dense forest canopies in subtropical forests
653 in Korea (Hong et al., 2019b), deciduous forest ecosystems (Goulden et al., 1996), and a mixed hardwood forest
654 ecosystem (Schmid et al., 2000).

655 Our ~~study reveals that urban forests make significant traces~~results emphasize the important role of air
656 ~~temperature~~forest management in enhancing carbon uptake and ~~CO₂ fluxes~~evaporative cooling despite their
657 ~~relatively small area~~the low vegetation fraction. Our key findings are that urban forests in East Asia are highly
658 influenced by the East Asian monsoon like natural forests in this region, but such influence is mitigated by
659 artificial irrigation and fertilization in urban forests. ~~In particular, our~~Our results emphasize the importance of
660 forest management for efficient carbon uptake and evaporative cooling despite the low vegetation fraction.
661 Furthermore, our observation study also indicates that caution in soil management is necessary to reduce CO₂
662 emissions in urban forests, mainly resulting from large soil organic carbon. ~~We also highlight that our~~
663 ~~statistical CO₂ flux partitioning is a promising method to improve our understanding of the~~
664 ~~carbon cycle in urban and suburban areas, and a more extensive study is required for validation~~
665 ~~in another geographical zone. and warm environment.~~

666
667 *Acknowledgment.* This research was supported by the Korea Meteorological Administration Research and
668 Development Program under Grant KMI2021-01610 and National Research Foundation of Korea Grant from the
669 Korean Government (MSIT) (NRF-2018R1A5A1024958). All data and codes are available in Lee et al. (2021)
670 and upon request to the corresponding author (jhong@yonsei.ac.kr / <https://eapl.yonsei.ac.kr>).

671

Appendix A. List of Abbreviation

<u>Abbreviation</u>	<u>Definitions</u>	<u>Abbreviation</u>	<u>Definitions</u>
<u>CBD</u>	<u>the Gangnam, Seocho, and Songpa observatories at central business district</u>	<u>RE</u>	<u>ecosystem respiration</u>
<u>E_B</u>	<u>CO₂ emission from buildings</u>	<u>SD</u>	<u>the Seongdong weather station</u>
<u>EC</u>	<u>eddy covariance</u>	<u>SEB</u>	<u>surface energy balance</u>
<u>EP</u>	<u>the Eunpyeong site</u>	<u>SFP</u>	<u>the Seoul Forest Park</u>
<u>E_R</u>	<u>CO₂ emission from vehicles on roads</u>	<u>T_{air}</u>	<u>the screen-level air temperature</u>
<u>ET</u>	<u>evapotranspiration</u>	<u>T_{air_CBD}</u>	<u>air temperature at the CBD regions</u>
<u>EVI</u>	<u>enhanced vegetation index</u>	<u>T_{air_SD}</u>	<u>air temperature at the SD</u>
<u>F_C</u>	<u>net CO₂ exchange</u>	<u>UHI</u>	<u>urban heat island</u>
<u>$F_{C,0}$</u>	<u>F_C at zero PAR</u>	<u>UHI_i</u>	<u>urban heat island intensity</u>
<u>GP</u>	<u>the Gimpo weather station</u>	<u>UHI_i^C</u>	<u>UHI_i at CBD</u>
<u>GPP</u>	<u>gross primary production</u>	<u>UHI_i^S</u>	<u>UHI_i at SFP</u>
<u>GPP_{sat}</u>	<u>potential rate of ecosystem CO₂ uptake</u>	<u>VPD</u>	<u>vapor pressure deficit</u>
<u>K_L</u>	<u>downward shortwave radiation</u>	<u>ΔT_{air}</u>	<u>$T_{air_CBD} - T_{air_SD}$</u>
<u>LCZ</u>	<u>local climate zone</u>	<u>ΔQ_S</u>	<u>the net storage heat flux</u>
<u>MAP</u>	<u>mean annual precipitation</u>	<u>ΔQ_A</u>	<u>the net heat advection</u>
<u>MAT</u>	<u>mean annual temperature</u>	<u>h_c</u>	<u>mean canopy height</u>
<u>NBE</u>	<u>net biome exchange of CO₂ ($RE - GPP$)</u>	<u>z_0</u>	<u>mean roughness length</u>
<u>P</u>	<u>precipitation</u>	<u>z_d</u>	<u>zero-plane displacement height</u>
<u>PAR</u>	<u>photosynthetic active radiation</u>	<u>z_m</u>	<u>measurement height</u>
<u>Q_E</u>	<u>latent heat flux</u>	<u>α</u>	<u>quantum yield efficiency</u>
<u>Q_F</u>	<u>anthropogenic heat flux</u>	<u>β</u>	<u>Bowen ratio ($= \sum Q_H / \sum Q_E$)</u>

Q_H	<u>sensible heat flux</u>	λ	<u>source area weighted road ratio</u>
Q^*	<u>net radiation</u>	λ_v	<u>Vegetation cover fraction</u>
Q_{10}	<u>the rate by which respiration is multiplied when temperature increases by 10°C</u>		

674

675 **References**

- 676 [Alekseychik, P., Mammarella, I., Karpov, D., Dengel, S., Terentieva, I., Sabrekov, A., Glagolev, M. and Lapshina,](#)
677 [E.: Net ecosystem exchange and energy fluxes measured with the eddy covariance technique in a western Siberian](#)
678 [bog. Atmospheric Chemistry and Physics, 17, 9333-9345, 2017.](#)
- 679 Awal M. A, Ohta T., Matsumoto K., Toba T., Daikoku K., Hattori S., and coauthors: Comparing the carbon
680 sequestration capacity of temperate deciduous forests between urban and rural landscapes in central Japan. Urban
681 Forestry & Urban Greening, 9(3), 261-270, 2010.
- 682 Bae, J., and Ryu, Y.: Spatial and temporal variations in soil respiration among different land cover types under
683 wet and dry years in an urban park. Landscape and Urban Planning, 167, 378–385, 2017.
- 684 Ballinas, M., and Barradas, V. L.: The urban tree as a tool to mitigate the urban heat island in Mexico City: A
685 simple phenomenological model. Journal of environmental quality, 45(1), 157-166, 2016.
- 686 [Balogun, A. A., Adegoke, J. O., Vezhapparambu, S., Mauder, M., McFadden, J. P. and Gallo, K.: Surface energy](#)
687 [balance measurements above an exurban residential neighbourhood of Kansas City, Missouri. Boundary-Layer](#)
688 [Meteorology. 133, 299-321, 2009.](#)
- 689 Bergeron, O., and Strachan, I. B.: CO₂ sources and sinks in urban and suburban areas of a northern mid-latitude
690 city. Atmospheric Environment, 45(8), 1564-1573, 2011.
- 691 Bonan, G. B.: Forests and climate change: forcings, feedbacks, and the climate benefits of forests. Science, 320,
692 1444-1449. 2008.
- 693 Bowler, D. E., Buyung-Ali, L., Knight, T. M., and Pullin, A. S.: Urban greening to cool towns and cities: A
694 systematic review of the empirical evidence. Landscape and Urban Planning, 97(3), 147-155, 2010.
- 695 Chang, C. R., Li, M. H., and Chang, S. D.: A preliminary study on the local cool-island intensity of Taipei city
696 parks. Landscape and Urban Planning, 80(4), 386-395, 2007.
- 697 [Chatterjee, S., Swain, C.K., Nayak, A.K., Chatterjee, D., Bhattacharyya, P., Mahapatra, S.S., Debnath, M.,](#)
698 [Tripathi, R., Guru, P.K. and Dhal, B.: Partitioning of eddy covariance-measured net ecosystem exchange of CO₂](#)
699 [in tropical lowland paddy. Paddy and Water Environment, 18, 623-636, 2020.](#)
- 700 Chiesura, A.: The role of urban parks for the sustainable city. Landscape and Urban Planning, 68(1), 129-138,
701 2004.
- 702 Christen, A.: Atmospheric measurement techniques to quantify greenhouse gas emissions from cities. Urban
703 Climate, 10, 241-260, 2014.
- 704 [Christen, A. and Vogt, R.: Energy and radiation balance of a central European city. International Journal of](#)
705 [Climatology. 24, 1395-1421, 2004.](#)
- 706 Coutts, A. M., Beringer, J., and Tapper, N. J.: Impact of increasing urban density on local climate: Spatial and
707 temporal variations in the surface energy balance in Melbourne, Australia. Journal of Applied Meteorology and
708 Climatology, 46(4), 477-493, 2007a.
- 709 Coutts, A. M., Beringer, J., and Tapper, N. J.: Characteristics influencing the variability of urban CO₂ fluxes in
710 Melbourne, Australia. Atmospheric Environment, 41(1), 51-62, 2007b.
- 711 Crawford, B., Grimmond, C. S. B., and Christen, A.: Five years of carbon dioxide fluxes measurements in a highly
712 vegetated suburban area. Atmospheric Environment, 45(4), 896-905, 2011.

713 Crawford, B., and Christen, A.: Spatial source attribution of measured urban eddy covariance CO₂ fluxes.
714 Theoretical and Applied Climatology, 119(3-4), 733-755, 2015.

715 ~~[Desai, A.R., Richardson, A.D., Moffat, A.M., Kattge, J., Hollinger, D.Y., Barr, A., Falge, E., Noormets, A., Papale,](#)~~
716 ~~[D., Reichstein, M. and Stauch, V.J.: Cross-site evaluation of eddy covariance GPP and RE decomposition](#)~~
717 ~~[techniques. Agricultural and Forest Meteorology, 148, 821-838, 2008.](#)~~

718

719 Emmel, C., D'Odorico, P., Reville, A., Hörtnagl, L., Ammann, C., Buchmann, N. and Eugster, W.: Canopy
720 photosynthesis of six major arable crops is enhanced under diffuse light due to canopy architecture. Global Change
721 Biology, 26(9), 2020.

722 Falge, E., Baldocchi, D., Olson, R., Anthoni, P., Aubinet, M., Bernhofer, C., Burba, G., Ceulemans, R., Clement,
723 R., Dolman, H., Granier, A., Gross, P., Grünwald, T., Hollinger, D., Jensen, N., Katul, G., Keronen, P., Kwalski,
724 A., Lai, C., Law, B., Meyers, T., Moncrieff, J., Moors, E., Munger, W., Pilegaard, K., Rannik, Ü., Rebmann, C.,
725 Suyker, A., Tenhunen, J., Tu, K., Verma, S., Vesala, T., Wilson, K., and Wofsy, S.: Gap filling strategies for long
726 term energy flux data sets. Agricultural and Forest Meteorology, 107, 71-77, 2001.

727 Feigenwinter, C., Vogt, R., and Christen, A.: Eddy covariance measurements over urban areas. In Eddy
728 Covariance (pp. 377-397). Springer, Dordrecht, 2012.

729 Feyisa, G. L., Dons, K., and Meilby, H.: Efficiency of parks in mitigating urban heat island effect: An example
730 from Addis Ababa. Landscape and Urban Planning, 123, 87-95, 2014.

731 ~~[Fratini, G., Ibrom, A., Arriga, N., Burba, G., and Papale, D.: Relative humidity effects on water vapour fluxes](#)~~
732 ~~[measured with closed path eddy covariance systems with short sampling lines. Agricultural and Forest](#)~~
733 ~~[Meteorology, 165, 53-63, 2012.](#)~~

734 ~~[Goldbach, A. and Kuttler, W.: Quantification of turbulent heat fluxes for adaptation strategies within urban](#)~~
735 ~~[planning. International Journal of Climatology, 33, 143-159, 2013.](#)~~

736 Goulden, M. L., Munger, J. W., Fan, S. M., Daube, B. C., and Wofsy, S. C.: Measurements of carbon sequestration
737 by long-term eddy covariance: Methods and a critical evaluation of accuracy. Global Change Biology, 2(3), 169-
738 182, 1996.

739 ~~[Grimmond, C. S. B. and Oke, T. R.: Comparison of heat fluxes from summertime observations in the suburbs of](#)~~
740 ~~[four North American cities. Journal of Applied Meteorology, 34, 873-889, 1995.](#)~~

741 ~~[Grimmond, C. S. B. and Oke, T. R.: Aerodynamic properties of urban areas derived from analysis of surface form.](#)~~
742 ~~[Journal of Applied Meteorology and Climatology, 38, 1262-1292, 1999.](#)~~

743 Haaland, C., and van Den Bosch, C. K.: Challenges and strategies for urban green-space planning in cities
744 undergoing densification: A review. Urban forestry & Urban Greening, 14(4), 760-771, 2015.

745 Hamada, S., and Ohta, T.: Seasonal variations in the cooling effect of urban green areas on surrounding urban
746 areas. Urban Forestry & Urban Greening, 9(1), 15-24, 2010.

747 Hansen, J., Ruedy, R., Sato, M., and Lo, K.: Global surface temperature change. Reviews of Geophysics, 48(4),
748 2010.

749 ~~[Hsieh, C. I., Katul, G., and Chi, T. W.: An approximate analytical model for footprint estimation of scalar fluxes](#)~~
750 ~~[in thermally stratified atmospheric flows. Advances in Water Resources, 23\(7\), 765-772, 2000.](#)~~

751 Hiller, R. V., McFadden, J. P., and Kljun, N.: Interpreting CO₂ fluxes over a suburban lawn: the influence of
752 traffic emissions. *Boundary-Layer Meteorology*, 138(2), 215-230, 2011.

753 Hong, J., and Kim, J.: Impact of the Asian monsoon climate on ecosystem carbon and water exchanges: a wavelet
754 analysis and its ecosystem modeling implications. *Global Change Biology*, 17(5), 1900-1916, 2011.

755 Hong, J., [Kwon, H., Lim, J., Byun, Y., Lee, J., and Kim, J.: Standardization of KoFlux eddy-covariance data](#)
756 [processing. Korean J. Agric. For. Meteorol., 11, 19-26, 2009.](#)

757 [Hong, J., Takagi, K., Ohta, T., and Kodama, Y.: Wet surface resistance of forest canopy in monsoon Asia:](#)
758 [Implications for eddy-covariance measurement of evapotranspiration. Hydrological Processes, 28\(1\), 37-42, 2014.](#)

759 Hong, J. W., Hong, J., Lee, S. E., and Lee, J.: Spatial distribution of urban heat island based on local climate zone
760 of automatic weather station in Seoul metropolitan area. *Atmosphere*, 23(4), 413-424, 2013.

761 Hong, J. W., and Hong, J.: Changes in the Seoul metropolitan area urban heat environment with residential
762 redevelopment. *Journal of Applied Meteorology and Climatology*, 55(5), 1091-1106, 2016.

763 Hong, J. W., Hong, J., Kwon, E. E., and Yoon, D.: Temporal dynamics of urban heat island correlated with the
764 socio-economic development over the past half-century in Seoul, Korea. *Environmental Pollution*, 254, 112934,
765 2019a.

766 Hong, J.-W., Hong, J., Chun, J., Lee, Y., Chang, L., Lee, J., Yi, K., Park, Y., Byun, B., and Joo, S.: Comparative
767 assessment of net CO₂ exchange across an urbanization gradient in Korea based on in situ observation, *Carbon*
768 *Balance and Management*, <https://doi.org/10.1186/s13021-019-0128-6>, 2019b.

769 Hong, J. W., Lee, S. D., Lee, K., and Hong, J.: Seasonal variations in the surface energy and CO₂ flux over a high-
770 rise, high-population, residential urban area in the East Asian monsoon region. *International Journal of*
771 *Climatology*, <https://doi.org/10.1002/joc.6463>, 2020.

772 ~~Horst, T. W., and Lenschow, D. H.: Attenuation of scalar fluxes measured with spatially displaced sensors.~~
773 ~~*Boundary Layer Meteorology*, 130(2), 275-300, 2009.~~

774

775 [Hsieh, C. I., Katul, G., and Chi, T. W.: An approximate analytical model for footprint estimation of scalar fluxes](#)
776 [in thermally stratified atmospheric flows. Advances in Water Resources, 23\(7\), 765-772, 2000.](#)

777 Kennedy, C. A., Ibrahim, N., and Hoornweg, D.: Low-carbon infrastructure strategies for cities. *Nature Climate*
778 *Change*, 4(5), 343, 2014.

779 Kent, C. W., Lee, K., Ward, H. C., Hong, J. W., Hong, J., Gatey, D., and Grimmond, S.: Aerodynamic roughness
780 variation with vegetation: analysis in a suburban neighbourhood and a city park. *Urban Ecosystems*, 21(2), 227-
781 243, 2018.

782 Khatun, R., Ohta, T., Kotani, A., Asanuma, J., Gamo, M., Han, S., Hirano, T., Nakai, Y., Saigusa, N., Takagi, K.
783 and Wang, H. (2011) Spatial variations in evapotranspiration over East Asian forest sites. I. Evapotranspiration
784 and decoupling coefficient. *Hydrological Research Letters*, 5, 83-87, 2011.

785 Kim, Y., Woo, S.K., Park, S., Kim, M. and Han, D.: A Study on Evaluation Methodology of Greenhouse Gas and
786 Air Pollutant Emissions on Road Network - Focusing on Evaluation Methodology of CO₂ and NO_x Emissions
787 from Road. Korea: The Korea Transport Institute (Annual Report), 2011.

788 Kirschbaum, M.U.F., Eamus, D., Gifford, R.M., Roxburgh, S.H. and Sands, P.J.: Definitions of some ecological
789 terms commonly used in carbon accounting. In Net Ecosystem Exchange Workshop, 18-20, 2001.

790 Kroeger, T., McDonald, R. I., Boucher, T., Zhang, P., and Wang, L.: Where the people are: Current trends and
791 future potential targeted investments in urban trees for PM10 and temperature mitigation in 27 US cities.
792 *Landscape and Urban Planning*, 177, 227-240, 2018.

793 Kordowski, K., and Kuttler, W.: Carbon dioxide fluxes over an urban park area. *Atmospheric Environment*, 44(23),
794 2722-2730, 2010.

795 Kwon, H., Park, T. Y., Hong, J., Lim, J. H., and Kim, J.: Seasonality of Net Ecosystem Carbon ~~Exchange~~
796 in Two Major Plant Functional Types in Korea. *Asia-Pacific Journal of Atmospheric Sciences*, 45(2), 149-163,
797 2009.

798 Lee, K. Energy, water and CO₂ exchanges in an artificially constructed urban forest, Master Degree Dissertation,
799 Yonsei University, Seoul, 2015.

800 Lee, K., Hong, J. W., Kim, J., and Hong, J.: Partitioning of net CO₂ exchanges at the city-atmosphere interface
801 into biotic and abiotic components. *MethodsX*, 8, 101231, 2021.

802 Lietzke, B., Vogt, R., Feigenwinter, C., and Parlow, E.: On the controlling factors for the variability of carbon
803 dioxide flux in a heterogeneous urban environment. *International Journal of climatology*, 35(13), 3921-3941, 2015.

804 Macdonald, R. W., Griffiths, R. F., and Hall, D. J.: An improved method for the estimation of surface roughness
805 of obstacle arrays. *Atmospheric Environment*, 32(11), 1857-1864, 1998.

806 Mahecha, M. D., Reichstein, M., Carvalhais, N., Lasslop, G., Lange, H., Seneviratne, S. I., Vargas, R., Ammann,
807 C., Arain, M. A., Cescatti, A., Janssens, I., Migliavacca, M., Montagnani, L., and Richardson, A.: Global
808 convergence in the temperature sensitivity of respiration at ecosystem level. *Science*, 329(5993), 838-840, 2010.

809 McCarthy, M. P., Best, M. J., and Betts, R. A.: Climate change in cities due to global warming and urban effects.
810 *Geophysical Research Letters*, 37(9), 2010.

811 Menzer, O., and McFadden, J. P.: Statistical partitioning of a three-year time series of direct urban net CO₂ flux
812 measurements into biogenic and anthropogenic components. *Atmospheric Environment*, 170, 319-333, 2017.

813 ~~Moncrieff, J., Clement, R., Finnigan, J., and Meyers, T.: Averaging, detrending, and filtering of eddy covariance~~
814 ~~time series. In Handbook of micrometeorology, Springer, Dordrecht, 2004.~~

815 Moriwaki, R., and Kanda, M.: Seasonal and diurnal fluxes of radiation, heat, water vapor, and carbon dioxide
816 over a suburban area. *Journal of Applied Meteorology*, 43(11), 1700-1710, 2004.

817 Munger, J. W., Loescher, H. W., and Luo, H.: Measurement, tower, and site design considerations. In *Eddy*
818 *Covariance* (pp. 21-58). Springer, Dordrecht, 2012.

819 Norton, B. A., Coutts, A. M., Livesley, S. J., Harris, R. J., Hunter, A. M., and Williams, N. S.: Planning for cooler
820 cities: A framework to prioritise green infrastructure to mitigate high temperatures in urban landscapes. *Landscape*
821 *and Urban Planning*, 134, 127-138, 2015.

822 Nowak, D. J.: Atmospheric carbon reduction by urban trees. *Journal of Environmental Management*, 37(3), 207-
823 217, 1993.

824 Nowak, D. J., Crane, D. E., Stevens, J. C., Hoehn, R. E., Walton, J. T., and Bond, J.: A ground-based method of
825 assessing urban forest structure and ecosystem services. *Aboriculture and Urban Forestry*. 34 (6): 347-358., 34(6),
826 2008.

827 Oke, T. R.: The energetic basis of the urban heat island. *Quarterly Journal of the Royal Meteorological Society*,
828 108(455), 1-24, 1982.

829 Oke, T. R.: The micrometeorology of the urban forest. *Philosophical Transactions of the Royal Society of London*.
830 B, *Biological Sciences*, 324(1223), 335-349, 1989.

831 Oke, T. R., Johnson, G. T., Steyn, D. G., and Watson, I. D.: Simulation of surface urban heat islands under 'ideal'
832 conditions at night part 2: Diagnosis of causation. *Boundary-Layer Meteorology*, 56(4), 339-358, 1991.

833 Oke, T.R., Mills, G., Christen, A., Voogt, J.A.: *Urban Climates*. Cambridge University Press, U.K., 2017.

834 Pastorello, G., Trotta, C., Canfora, E., Chu, H., Christianson, D., Cheah, Y. W., Poindexter, C., Chen,
835 J., Elbashandy, A., Humphrey, M., Isaac, P., Polidori, D., Ribeca, A., van Ingen, C., Zhang, L., Amiro,
836 B., Ammann, C., Arain, M.A., Ardö, J., Arkebauer, T., Arndt, S.K., Arriga, N., Aubinet, M., Aurela,
837 M., Baldocchi, D., Barr, A., Beamesderfer, E., Marchesini, L.B., Bergeron, O., Beringer, J., Bernhofer,
838 C., Berveiller, D., Billesbach, D., Black, T.A., Blanken, P.D., Bohrer, G., Boike, J., Bolstad, P.V., Bonal,
839 D., Bonnefond, J.-M., Bowling, D.R., Bracho, R., Brodeur, J., Brümmer, C., Buchmann, N., Burban, B., Burns,
840 S.P., Buysse, P., Cale, P., Cavagna, M., Cellier, P., Chen, S., Chini, I. Christensen, T.R., Cleverly, J., Collalti,
841 A., Consalvo, C., Cook, B.D., Cook, D., Coursolle, C., Cremonese, E., Curtis, P.S., D'Andrea, E., da Rocha,
842 H., Dai, X., Davis, K.J., De Cinti, B., de Grandcourt, A., De Ligne, A., De Oliveira, R.C., Delpierre, N., Desai,
843 A.R., Di Bella, C.M., di Tommasi, P., Dolman, H., Domingo, F., Dong, G., Dore, S., Duce, P., Dufrêne, E., Dunn,
844 A., Dušek, J., Eamus, D., Eichelmann, U., ElKhidir, H.A.M., Eugster, W., Ewenz, C.M., Ewers, B., Famulari,
845 D., Fares, S., Feigenwinter, I., Feitz, A., Fensholt, R., Filippa, G., Fischer, M., Frank, J., Galvagno, M., Gharun,
846 M., Gianelle, D., Gielen, B., Gioli, B., Gitelson, A., Goded, I., Goeckede, M., Goldstein, A.H., Gough,
847 C.M., Goulden, M.L., Graf, A., Griebel, A., Gruening, C., Grünwald, T., Hammerle, A., Han, S., Han,
848 X., Hansen, B.U., Hanson, C., Hatakka, J., He, Y., Hehn, M., Heinesch, B., Hinko-Najera, N., Hörtnagl,
849 L., Hutley, L., Ibrom, A., Ikawa, H., Jackowicz-Korczynski, M., Janouš, D., Jans, W., Jassal, R., Jiang, S., Kato,
850 T., Khomik, M., Klatt, J., Knohl, A., Knox, S., Kobayashi, H., Koerber, G., Kolle, O., Kosugi, Y., Kotani,
851 A., Kowalski, A., Kruijt, B., Kurbatova, J., Kutsch, W.L., Kwon, H., Launiainen, S., Laurila, T., Law,
852 B., Leuning, R., Li, Y., Liddell, M., Limousin, J.-M., Lion, M., Liska, A.J., Lohila, A., López-Ballesteros,
853 A., López-Blanco, E., Loubet, B., Loustau, D., Lucas-Moffat, A., Lüers, J., Ma, S., Macfarlane, C., Magliulo,
854 V., Maier, R., Mammarella, I., Manca, G., Marcolla, B., Margolis, H.A., Marras, S., Massman, W., Mastepanov,
855 M., Matamala, R., Matthes, J.H., Mazzenga, F., McCaughey, H., McHugh, I., McMillan, A.M.S., Merbold,
856 L., Meyer, W., Meyers, T., Miller, S.D., Minerbi, S., Moderow, U., Monson, R.K., Montagnani, L., Moore,
857 C.E., Moors, E., Moreaux, V., Moureaux, C., Munger, J.W., Nakai, T., Neiryneck, J., Nesic, Z., Nicolini,
858 G., Noormets, A., Northwood, M., Noretto, M., Nouvellon, Y., Novick, K., Oechel, W., Olesen, J.E., Ourcival,
859 J.-M., Papuga, S.A., Parmentier, F.-J., Paul-Limoges, E., Pavelka, M., Peichl, M., Pendall, E., Phillips,
860 R.P., Pilegaard, K., Pirk, N., Posse, G., Powell, T., Prasse, H., Prober, S.M., Rambal, S., Rannik, Ü., Raz-Yaseef,
861 N., Reed, D., de Dios, V.R., Restrepo-Coupe, N., Reverter, B.R., Roland, M., Sabbatini, S., Sachs, T., Saleska,

862 S.R., Sánchez-Cañete, E.P., Sanchez-Mejia, Z.M., Schmid, H.P., Schmidt, M., Schneider, K., Schrader,
863 F., Schroder, I., Scott, R.L., Sedlák, P., Serrano-Ortíz, P., Shao, C., Shi, P., Shironya, I., Siebicke, L., Šigut,
864 L., Silberstein, R., Sirca, C., Spano, D., Steinbrecher, R., Stevens, R.M., Sturtevant, C., Suyker, A., Tagesson,
865 T., Takanashi, S., Tang, Y., Tapper, N., Thom, J., Tiedemann, F., Tomassucci, M., Tuovinen, J.-P., Urbanski,
866 S., Valentini, R., van der Molen, M., van Gorsel, E., van Huissteden, K., Varlagin, A., Verfaillie, J., Vesala,
867 T., Vincke, C., Vitale, D., Vygodskaya, N., Walker, J.P., Walter-Shea, E., Wang, H., Weber, R., Westermann,
868 S., Wille, C., Wofsy, S., Wohlfahrt, G., Wolf, S., Woodgate, W., Li, Y., Zampedri, R., Zhang, J., Zhou, G., Zona,
869 D., Agarwal, D., Biraud, S., Torn, M., and Papale, D.: The FLUXNET2015 dataset and the ONEFlux processing
870 pipeline for eddy covariance data. *Scientific Data*, 7(1), 1-27, 2020.

871 Pataki, D. E., Bowling, D. R., and Ehleringer, J. R.: Seasonal cycle of carbon dioxide and its isotopic composition
872 in an urban atmosphere: Anthropogenic and biogenic effects. *Journal of Geophysical Research: Atmospheres*, 108,
873 D23, <https://doi.org/10.1029/2003JD003865>, 2003.

874 Peters, E. B., and McFadden, J. P.: Continuous measurements of net CO₂ exchange by vegetation and soils in a
875 suburban landscape. *Journal of Geophysical Research: Biogeosciences*, 117, G3,
876 <https://doi.org/10.1029/2011JG001933>, 2012.

877 Piao, S., Luyssaert, S., Ciais, P., Janssens, I. A., Chen, A., Cao, C., Fang, J., Friedlingstein, P., Luo, Y., and Wang,
878 S.: Forest annual carbon cost: A global-scale analysis of autotrophic respiration. *Ecology*, 91(3), 652-661, 2010.

879 Rahmstorf, S., and Coumou, D.: Increase of extreme events in a warming world. *Proceedings of the National
880 Academy of Sciences*, 108(44), 17905-17909, 2011.

881 Randerson, J.T., Chapin III, F.S., Harden, J.W., Neff, J.C. and Harmon, M.E.: Net ecosystem production: a
882 comprehensive measure of net carbon accumulation by ecosystems. *Ecological Applications*, 12(4), 937-947,
883 2002.

884 Raupach, M. R., Antonia, R. A., and Rajagopalan, S.: Rough-wall turbulent boundary layers, *Applied Mechanics
885 Reviews*, 44(1), 1-25, 1991.

886 Rowntree, R. A., and Nowak, D. J.: Quantifying the role of urban forests in removing atmospheric carbon dioxide.
887 *Journal of Arboriculture*. 17 (10): 269-275., 17(10), 1991.

888 Roy, S., Byrne, J., and Pickering, C.: A systematic quantitative review of urban tree benefits, costs, and assessment
889 methods across cities in different climatic zones. *Urban Forestry and Urban Greening*, 11(4), 351-363, 2012.

890 Schmid, H. P., Grimmond, C. S. B., Copley, F., Offerle, B., and Su, H. B.: Measurements of CO₂ and energy
891 fluxes over a mixed hardwood forest in the mid-western United States. *Agricultural and Forest Meteorology*,
892 103(4), 357-374, 2000.

893 Schmid, H. P., Su, H. B., Vogel, C. S., and Curtis, P. S.: Ecosystem-atmosphere exchange of carbon dioxide over
894 a mixed hardwood forest in northern lower Michigan. *Journal of Geophysical Research: Atmospheres*, 108(D14),
895 2003.

896 Shashua-Bar, L., and Hoffman, M. E.: Vegetation as a climatic component in the design of an urban street: An
897 empirical model for predicting the cooling effect of urban green areas with trees. *Energy and Buildings*, 31(3),
898 221-235, 2000.

899 Shim, C., J. Hong, J. Hong, Y. Kim, M. Kang, B. Thakuri, Y. Kim, J. Chun: Evaluation of MODIS GPP over a
900 complex ecosystem in East Asia: A case of Gwangneung flux tower in Korea, *Advances in Space Research*, 54,
901 2296-2308, 2014.

902 Spronken-Smith, R. A., Oke, T. R., and Lowry, W. P.: Advection and the surface energy balance across an
903 irrigated urban park. *International Journal of Climatology: A Journal of the Royal Meteorological Society*, 20(9),
904 1033-1047. 2000.

905 Stagakis, S., Chrysoulakis, N., Spyridakis, N., Feigenwinter, C., and Vogt, R.: Eddy Covariance measurements
906 and source partitioning of CO₂ emissions in an urban environment: Application for Heraklion, Greece.
907 *Atmospheric Environment*, 201, 278-292, 2019.

908 Stewart, I. D.: A systematic review and scientific critique of methodology in modern urban heat island literature.
909 *International Journal of Climatology*, 31(2), 200-217, 2011.

910 Stewart, I. D., and Oke, T. R.: Local climate zones for urban temperature studies. *Bulletin of the American*
911 *Meteorological Society*, 93(12), 1879-1900, 2012.

912 Stoy, P. C., Katul, G. G., Siqueira, M. B., Juang, J. Y., Novick, K. A., Uebelherr, J. M., and Oren, R.: An evaluation
913 of models for partitioning eddy covariance-measured net ecosystem exchange into photosynthesis and respiration.
914 *Agricultural and Forest Meteorology*, 141(1), 2-18, 2006.

915 Suyker, A.E. and Verma, S.B.: Interannual water vapor and energy exchange in an irrigated maize-based
916 agroecosystem. *Agricultural and Forest Meteorology*, 148, 417-427, 2008.

917 Takashi, S., Kosugi, Y., Tanaka, Y., Yano, M., Katayama, T., Tanaka, H., and Tani, M.: CO₂ exchange in a
918 temperate Japanese cypress forest compared with that in a cool-temperate deciduous broad-leaved forest.
919 *Ecological Research*, 20(3), 313-324, 2005.

920 Ueyama, M., and Ando, T.: Diurnal, weekly, seasonal, and spatial variabilities in carbon dioxide flux in different
921 urban landscapes in Sakai, Japan. *Atmospheric Chemistry and Physics*, 16(22), 14727-14740, 2016.

922 United Nations, Department of Economic and Social Affairs, Population Division: *World Urbanization Prospects:*
923 *The 2018 Revision (ST/ESA/SER.A/420)*. New York: United Nations, 2019.

924 Velasco, E., and Roth, M.: Cities as net sources of CO₂: Review of atmospheric CO₂ exchange in urban
925 environments measured by eddy covariance technique. *Geography Compass*, 4(9), 1238-1259, 2010.

926 Velasco, E., Roth, M., Tan, S. H., Quak, M., Nabarro, S. D. A., and Norford, L.: The role of vegetation in the
927 CO₂ flux from a tropical urban neighbourhood, *Atmospheric Chemistry and Physics*, 13, 10185–10202,
928 <https://doi.org/10.5194/acp-13-10185-2013>, 2013.

929 Velasco, E., Roth, M., Norford, L., and Molina, L. T.: Does urban vegetation enhance carbon sequestration?,
930 *Landscape and Urban Planning*, 148, 99-107, 2016.

931 ~~Viekers, D., and Mahrt, L.: Quality control and flux sampling problems for tower and aircraft data. *Journal of*~~
932 ~~*Atmospheric and Oceanic Technology*, 14(3), 512-526, 1997.~~

933 Wang, L., Lee, X., Schultz, N., Chen, S., Wei, Z., Fu, C., Gao, Y., Yang, Y., and Lin, G.: Response of surface
934 temperature to afforestation in the Kubuqi Desert, Inner Mongolia. *Journal of Geophysical Research:*
935 *Atmospheres*, 123, 948-964, 2018.

936 Ward, H. C., Evans, J. G., and Grimmond, C. S. B.: Multi-season eddy covariance observations of energy, water
937 and carbon fluxes over a suburban area in Swindon, UK. *Atmospheric Chemistry and Physics*, 13(9), 4645-4666,
938 2013.

939 Ward, H. C., Kotthaus, S., Grimmond, C. S. B., Bjoergegren, A., Wilkinson, M., Morrison, W. T. J., Evans, J. G.,
940 Morrison, J. I. L. M and Iamarino, M.: Effects of urban density on carbon dioxide exchanges: Observations of dense
941 urban, suburban and woodland areas of southern England. *Environmental Pollution*, 198, 186-200, 2015.

942 Weissert, L. F., Salmond, J. A., and Schwendenmann, L.: A review of the current progress in quantifying the
943 potential of urban forests to mitigate urban CO₂ emissions. *Urban Climate*, 8, 100-125, 2014.

944 [York D., Evensen N., Martinez M., and Delgado J.: Unified equations for the slope, intercept, and standard errors](#)
945 [of the best straight line. *American Journal of Physics*, 72\(3\), 367-375, 2004.](#)

946 Yu, C., and Hien, W. N.: Thermal benefits of city parks. *Energy and Buildings*, 38(2), 105-120, 2006.

947

948

949 Table 1. Details of the stations used in this study.

Sites	Location	<u>LCZ</u> Local climate zone	<u>Height</u> <u>[m]</u> Measurement <u>height (m)</u>
<u>Eddy covariance station</u>			
SFP (Seoul Forest Park)	37.5446°N, 127.0379°E	<u>Dense tree (LCZ_A)</u>	12.2
EP (Eunpyeong)	37.6350°N, 126.9287°E	<u>Compact highrise (LCZ₁)</u>	30
<u>Automatic weather station</u>			
SD (Seongdong)	37.5472°N, 127.0389°E	<u>Open midrise and scatted trees</u> <u>(LCZ_{5B})</u>	25
<u>AVG</u> <u>CBD</u>		<u>Compact midrise and highrise</u>	<u>59</u>
(Gangnam)	37.5134°N, 127.0467°E	<u>(LCZ₂₁)</u>	<u>35.5</u>
(Seocho)	37.4889°N, 127.0156°E	<u>LCZ₂₁</u>	<u>58.220</u>
(Songpa)	37.5115°N, 127.0967°E	<u>LCZ₁₅ Compact highrise and</u> <u>open midrise (LCZ₁₅)</u>	<u>13</u> <u>43</u>
<u>Aerodrome meteorological observation station</u>			
GP (Gimpo)	37.5722°N, 126.7751°E	<u>Low plants (LCZ_D)</u>	<u>41.41.5</u>

950

951

952 Table 2. ~~Gap filled annual budgets for surface energy fluxes~~ Daytime Bowen ratio ($\beta = Q_H/Q_E$) in summer at the
 953 ~~SFP and precipitation (P)~~ other urban sites of the similar vegetation cover fraction (λ_v).

<u>Site name</u>	<u>β</u>	<u>λ_v</u>	<u>References</u>
<u>SFP</u>	<u>0.56</u>	<u>0.57</u>	<u>this study</u>
<u>Sites Basel-Sperrstrasse</u>	<u>Q_H</u> <u>(MJ m⁻²) 2.5</u>	<u>Q_E</u> <u>(MJ m⁻²) 0.16</u>	<u>Q^*</u> <u>(MJ m⁻²) Christen and Vogt (2004)</u>
<u>Basel-Spalenring</u>	<u>2.3</u>	<u>0.32</u>	<u>Christen and Vogt (2004)</u>
<u>Tucson</u>	<u>1.8</u>	<u>0.42</u>	<u>Grimmond and Oke (1995)</u>
<u>Sacramento</u>	<u>1.4</u>	<u>0.42</u>	<u>Grimmond and Oke (1995)</u>
<u>Chicago</u>	<u>0.8</u>	<u>0.44</u>	<u>Grimmond and Oke (1995)</u>
<u>Los Angeles</u>	<u>1.4</u>	<u>0.41</u>	<u>Grimmond and Oke (1995)</u>
<u>Kansas City</u>	<u>0.48</u>	<u>0.58</u>	<u>Balogun et al. (2009)</u>
<u>Oberhausen-suburban</u>	<u>0.36</u>	<u>0.69</u>	<u>Goldbach and Kuttler (2013)</u>

954

955

956

Table 3. Gap-filled annual budgets for surface energy fluxes and precipitation (P).

	<u>ET</u> (mm)	<u>Q_H</u> (MJ m ⁻²)	<u>Q_E</u> (MJ m ⁻²)	<u>Q*</u> (MJ m ⁻²)	<u>P</u> (mm)
1 st year (2013.06 – 2014.05)	367	726	896	1797	1256
2 nd year (2014.06 – 2015.05)	320	867	781	1848	932
Mean annual sum of two-year	344	797	839	1823	1094

957

958

959 Table 34. Gap-filled annual budgets for F_C (observed by EC measurement) and its components, indicating
 960 ecosystem respiration (RE), photosynthetic uptake by vegetation (GPP), vehicle emissions (E_R), and building
 961 emissions (E_B). All fluxes are in $\text{kg CO}_2 \text{ m}^{-2} \text{ year}^{-1}$.

<u>Sites</u>	<u>F_C</u>	<u>RE</u>	<u>GPP</u>	<u>E_R</u>	<u>E_B</u>
<u>1st year</u> <u>(2013.06 – 2014.05)</u>	<u>6.6</u>	<u>5.1</u> <u>(77%)</u>	<u>4.7</u> <u>(70%)</u>	<u>5.4</u> <u>(81%)</u>	<u>1.0</u> <u>(15%)</u>
<u>2nd year</u> <u>(2014.06 – 2015.05)</u>	<u>7.6</u>	<u>5.0</u> <u>(65%)</u>	<u>4.5</u> <u>(59%)</u>	<u>5.4</u> <u>(71%)</u>	<u>1.9</u> <u>(25%)</u>
<u>Mean annual sum of two-year</u>	<u>7.1</u>	<u>5.1</u> <u>(71%)</u>	<u>4.6</u> <u>(64%)</u>	<u>5.4</u> <u>(76%)</u>	<u>1.5</u> <u>(20%)</u>

962

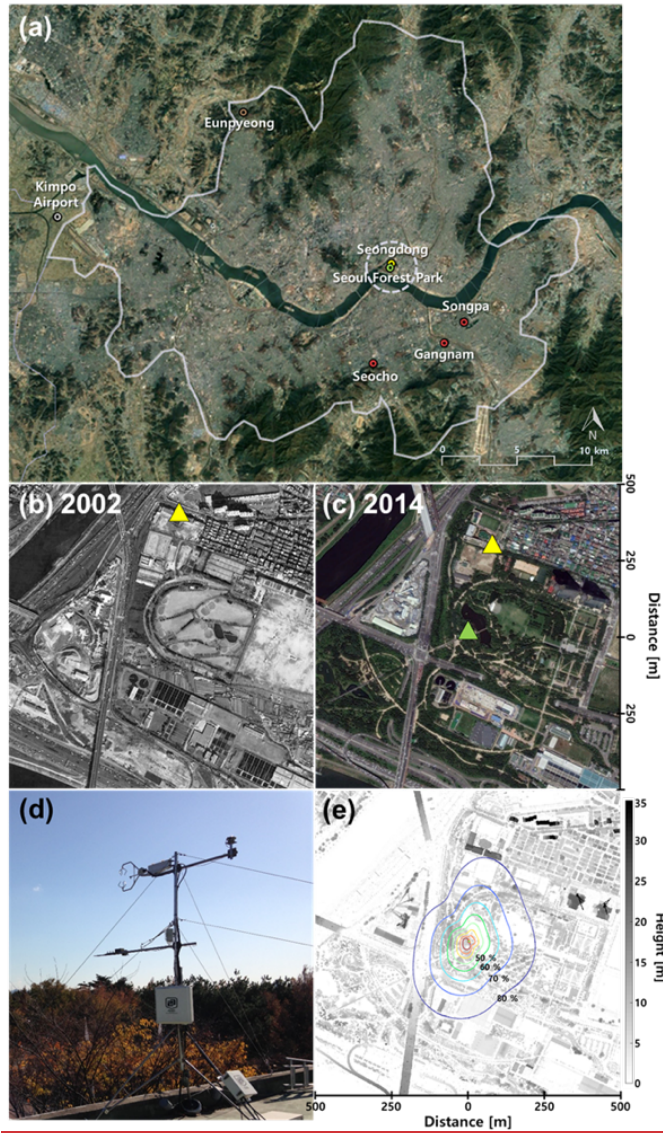
963

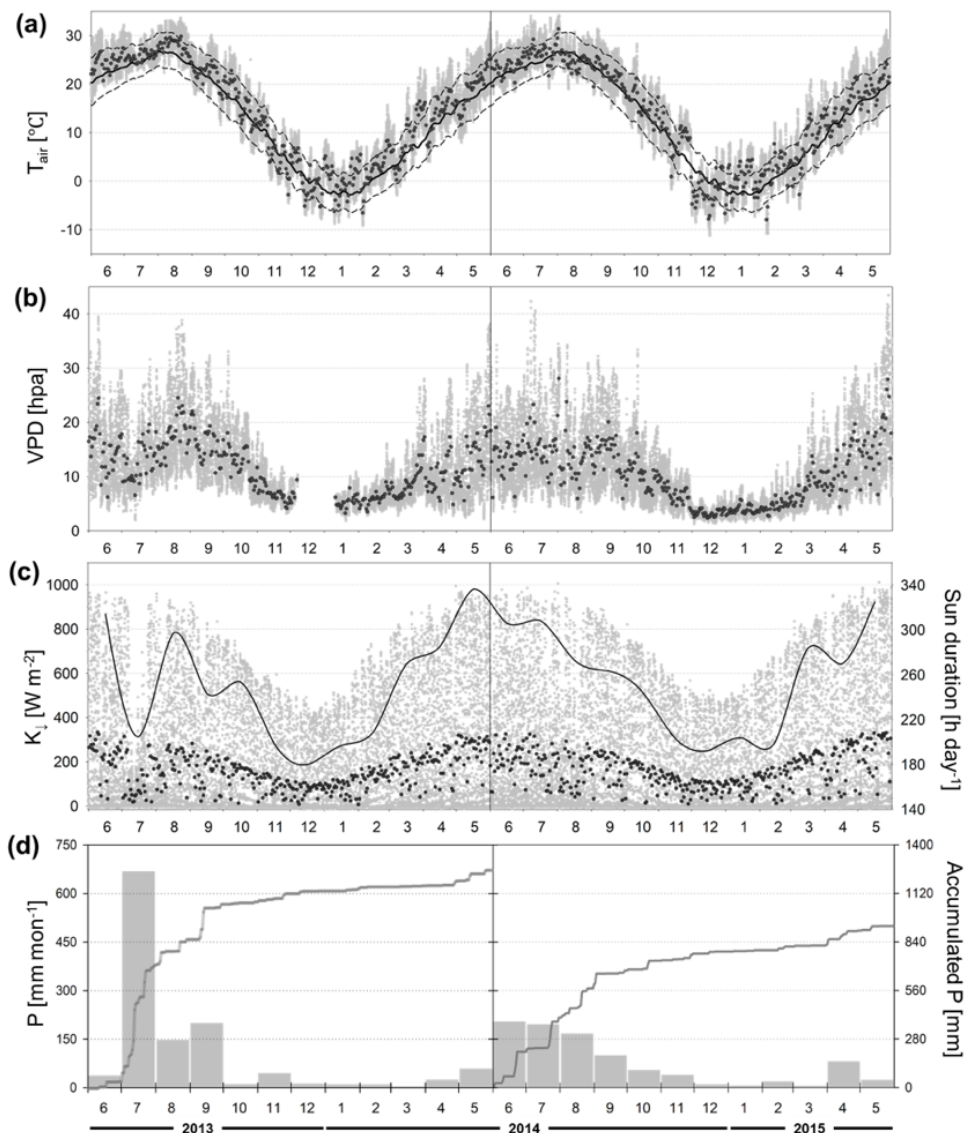
964 Table 45. Annual budgets of biogenic F_C components and ratios in deciduous broadleaf forests in similar climatic
 965 conditions reported in previous studies. All fluxes are in $\text{kg CO}_2 \text{ m}^{-2} \text{ year}^{-1}$.

SitesSite name	Reference	MAT (°C)	MAP (mm)	maximum LAI	RE	GPP	NBE	RE/GPP
Seoul Forest Park	This study	13.9	1094	1.6	5.1	4.6	+0.5	1.11
Nagoya urban forest	Awal et al. (2010)	15.9	1680	5.5	4.9	6.2	-1.3	0.74
Toyota rural forest		14.5	1518	4.5	2.6	4.6	-2.0	0.56
Gwangneung deciduous forest	Kwon et al. (2010)	12.8	1487	5	3.8	4.1	-0.3	0.93
Kiryu Experimental Watershed	Takanashi et al. (2005)	14.1	1309	5.5	3.9	5.6	-1.7	0.70
FLUXNET2015 dataset*	Pastorello et al. (2020)	14.5	1113		4.1	6.0	-1.9	0.68

966 *Average value of 8-year data from 4 sites having mean annual temperature (MAT) of 12-16°C, mean annual
 967 precipitation (MAP) of 900-2000 mm.

968





970

Figure 1.

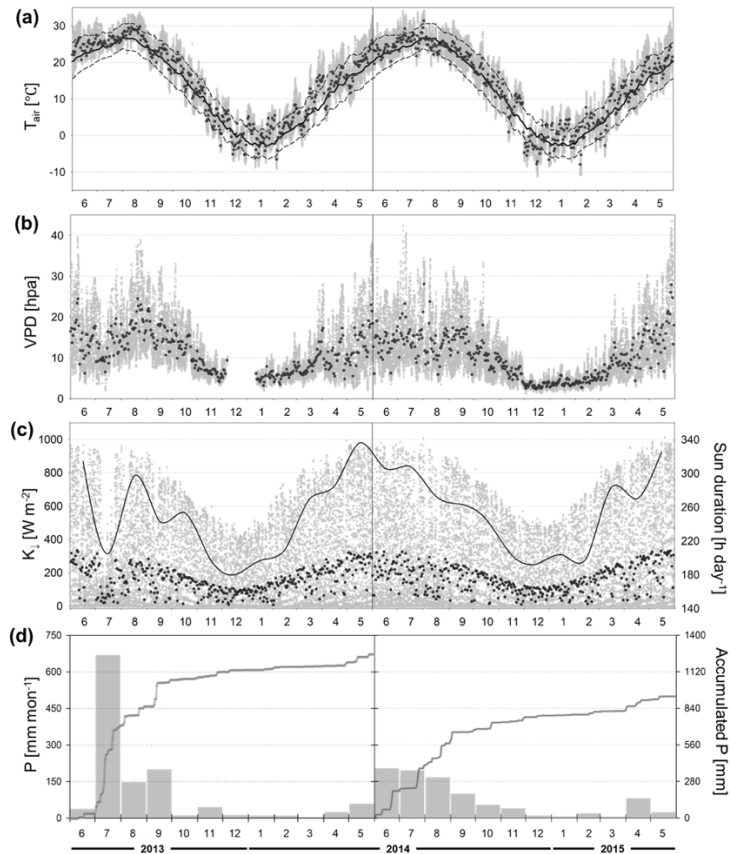
971

972

973

974

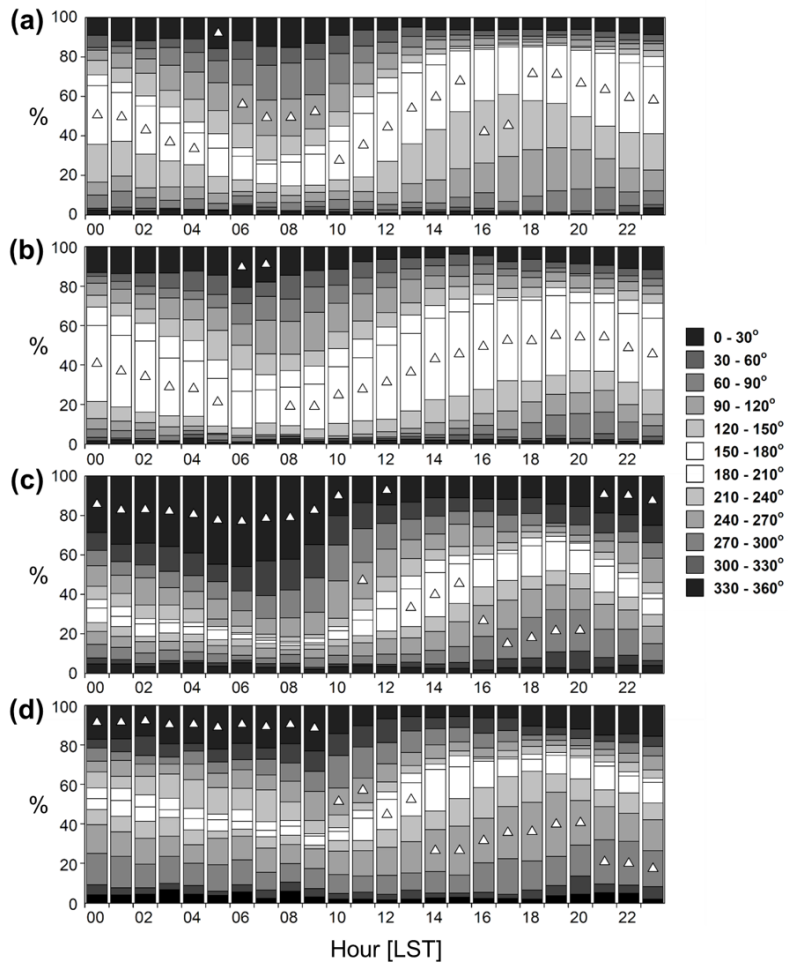
Figure 1. Site descriptions. (a) Location of the stations in Seoul (modified from map data © Google Earth 2019), (b) aerial photographs around Seoul Forest Park (SFP) in 2002 before the creation of the park and (c) in 2014 during the observation period (SFP; green triangle, SD; yellow triangle), (d) photograph of the SFP station, and (e) footprint climatology (Hsieh et al., 2000) with the height of surrounding obstacles around the SFP station.



975

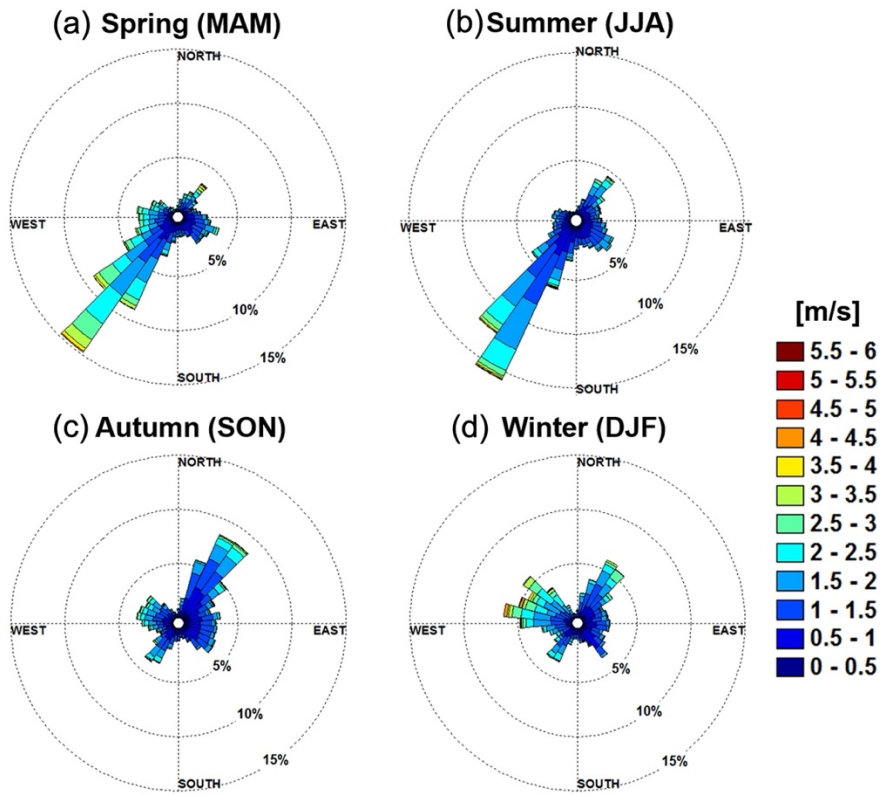
976 **Figure 2.** Climatic conditions of the SFP for two years from June 2013 to May 2015: 30-min (*gray dots*) and daily
 977 mean (*black dots*) (a) air temperature with 30-year normal values of Seoul (daily mean; *solid line*, min and max;
 978 *dashed lines*), (b) vapor pressure deficit (VPD) and missing data existing on December 2013, (c) downward
 979 shortwave radiation (K_t) and monthly averaged sunshine duration per day (*black line*), (d) monthly precipitation
 980 (*gray bars*) and yearly accumulated precipitation (*solid line*).

981



983
984

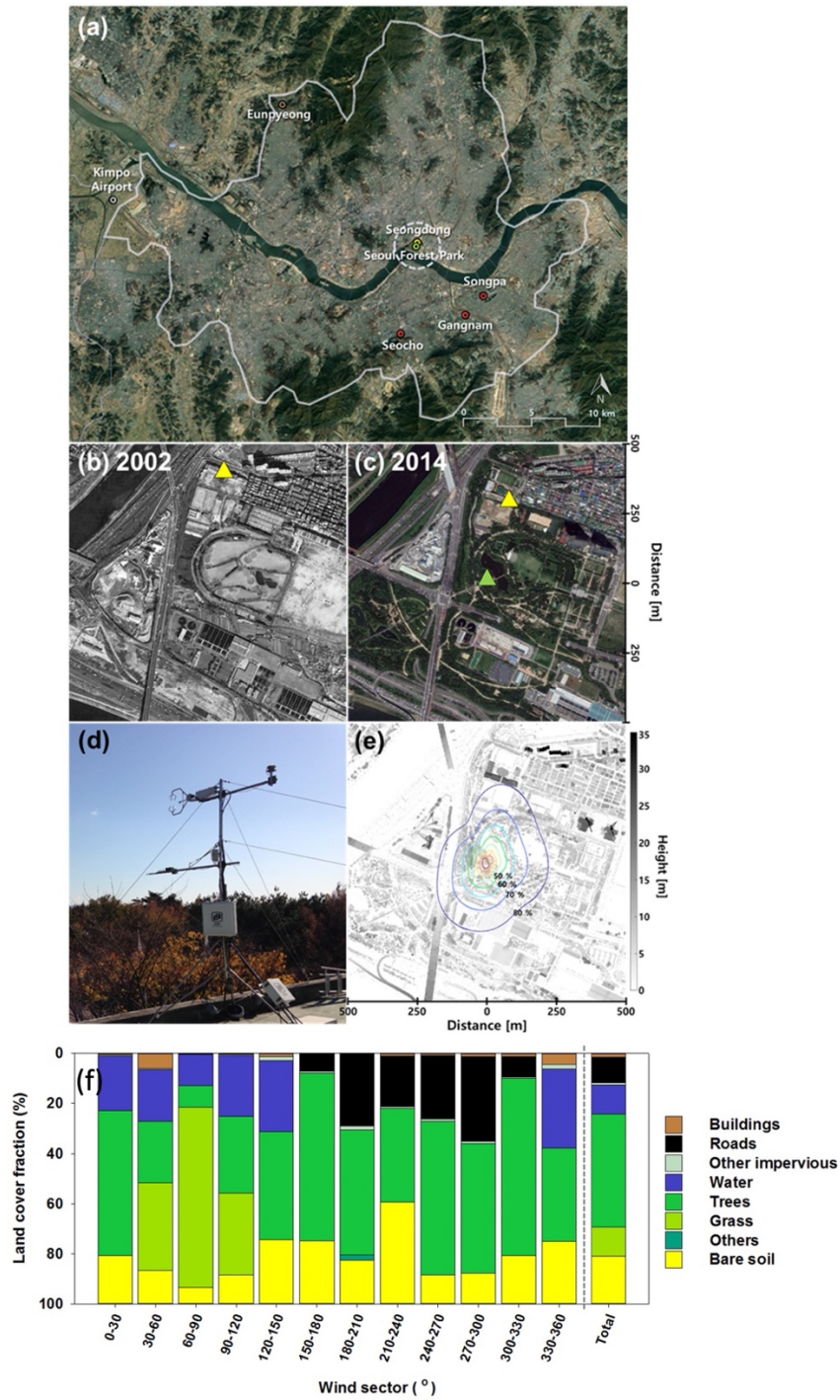
Figure 3. Seasonal mean diurnal courses of wind direction for 30° intervals. Each column represents the hourly ratio of the wind direction of the season



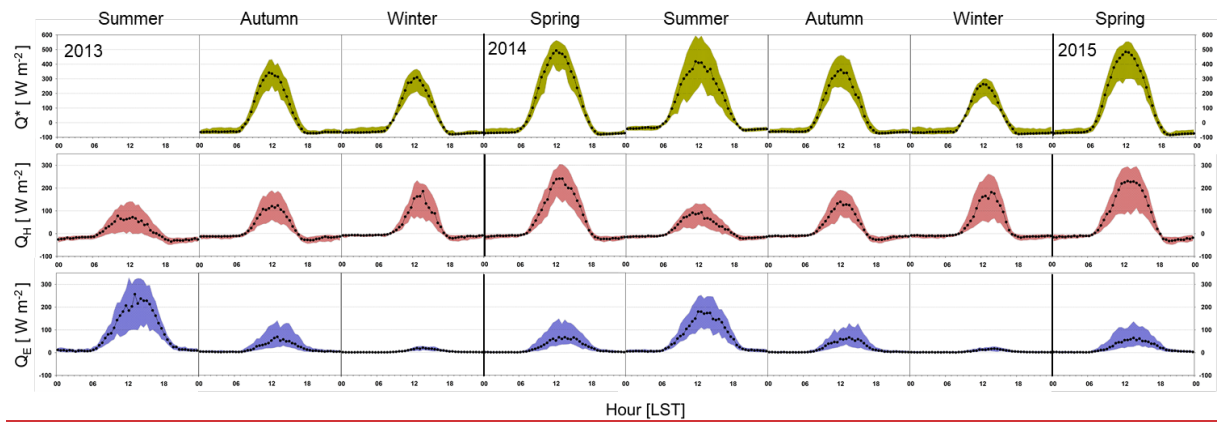
985
986

Figure 2. Wind roses with seasons: (a) spring (b) summer (c) autumn (d) winter. The white triangle indicates the dominant wind direction during that hour.

989

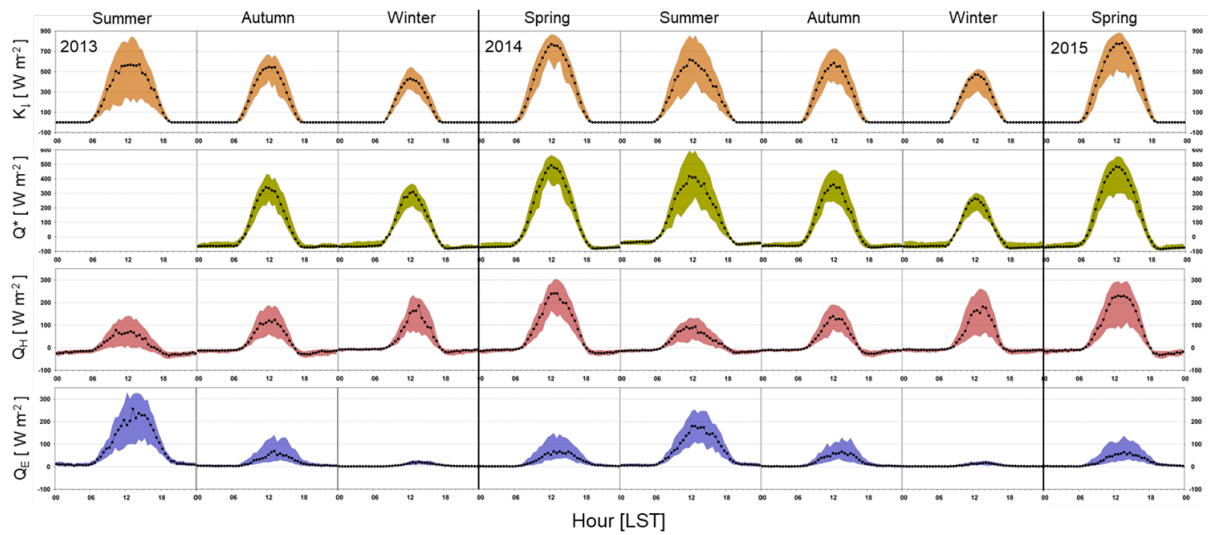


992 **Figure 3.** Site descriptions. (a) Location of the stations in Seoul (modified from map data ©
 993 Google Earth 2019), (b) aerial photographs around Seoul Forest Park (SFP) in 2002 before the
 994 creation of the park and (c) in 2014 during the observation period (SFP; *green triangle*, SD;
 995 *yellow triangle*), (d) photograph of the SFP station.



996
997
998

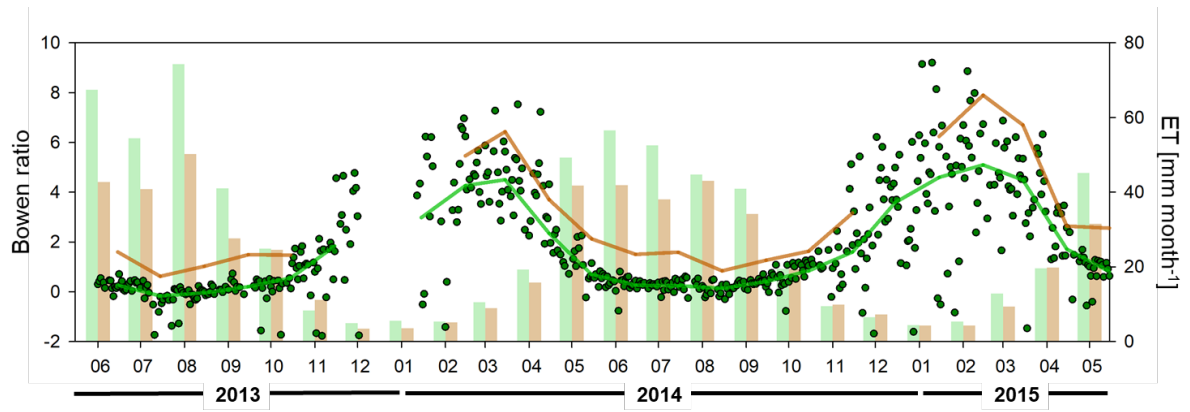
(e) footprint climatology (Hsieh et al., 2000) with the height of surrounding obstacles around the SFP station, and
(f) land cover fraction within a 150 m radius around a flux tower.



999

1000 Figure 4. Diurnal variations of surface energy fluxes. Seasonal median diurnal variations (*points*) and interquartile
 1001 ranges (*shaded*) of 30-min downward shortwave radiation (K_i), net radiation (Q^*), sensible heat flux (Q_H), and
 1002 latent heat flux (Q_E), and net radiation (Q^*) for two years. Since the net radiation system was installed in
 1003 September 2013, there was no Q^* value in the first summer.

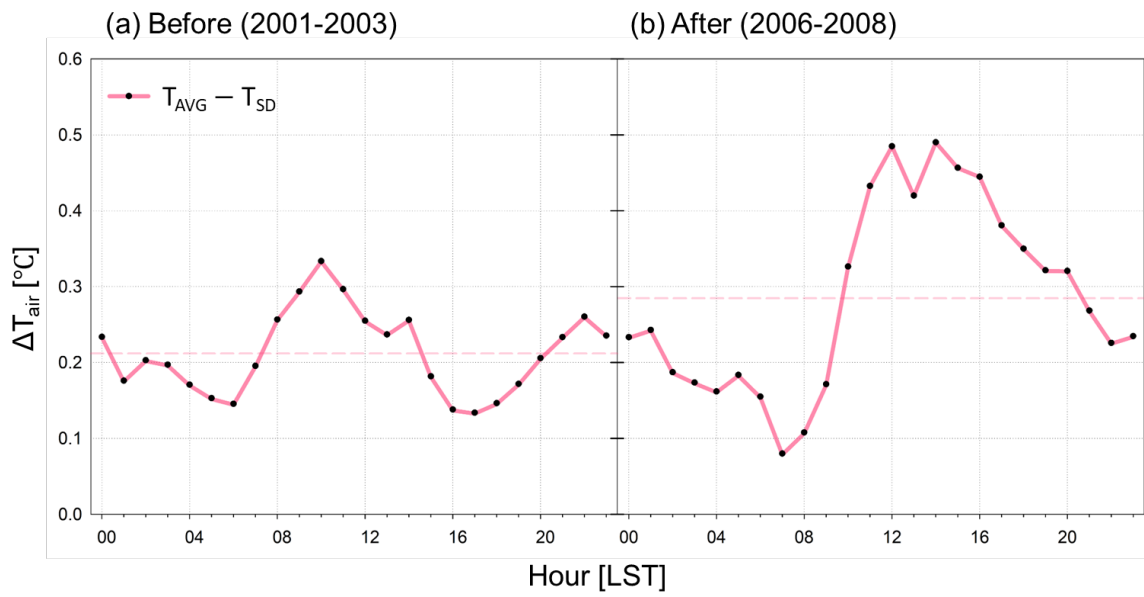
1004



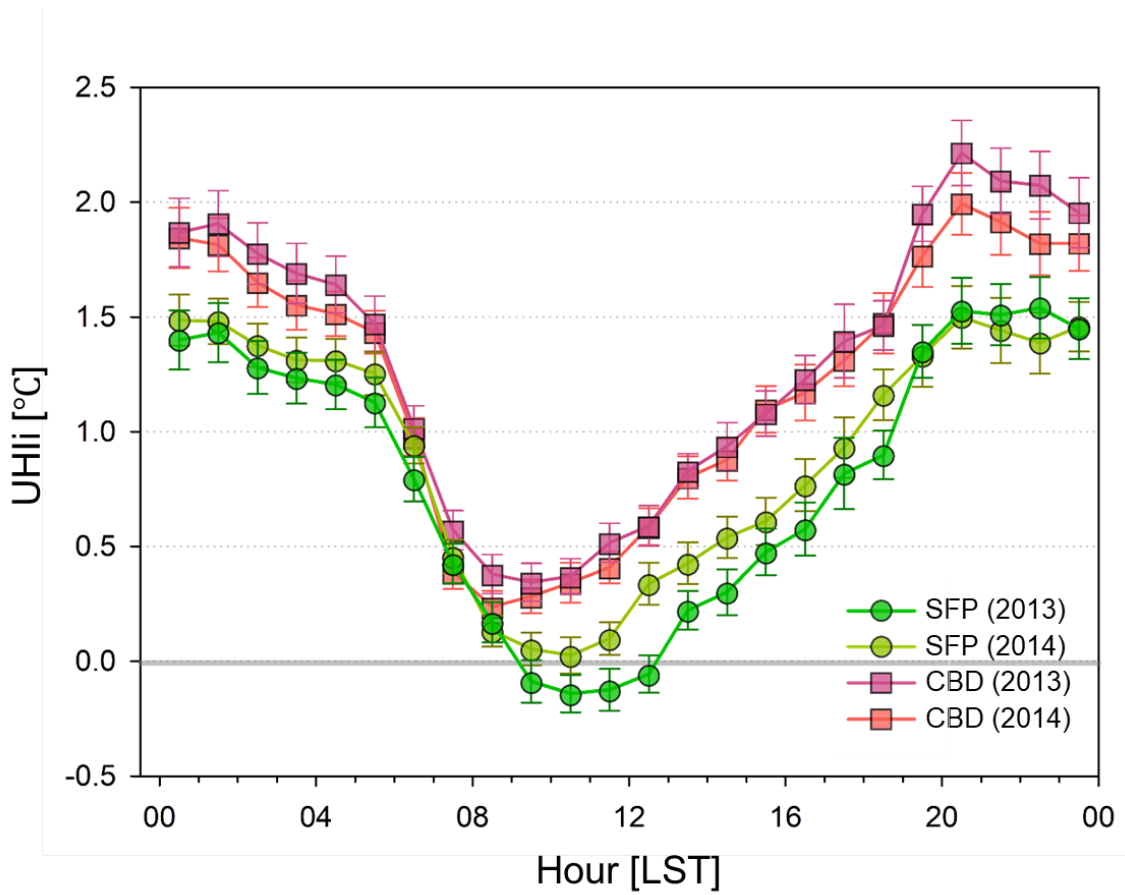
1005

1006 Figure 5. Daily Bowen ratio ($\beta = \sum Q_H / \sum Q_E$; dots), monthly Bowen ratio (lines), and gap-filled monthly
 1007 evapotranspiration (ET; bars) for two years (SFP; green, EP; brown).

1008



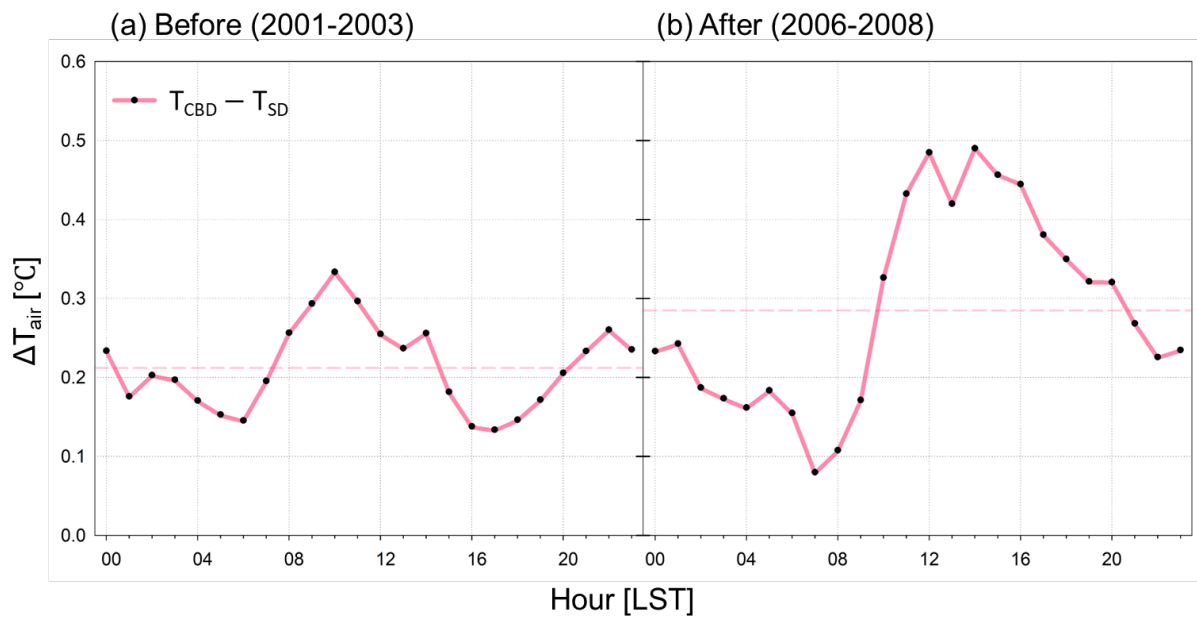
009



010

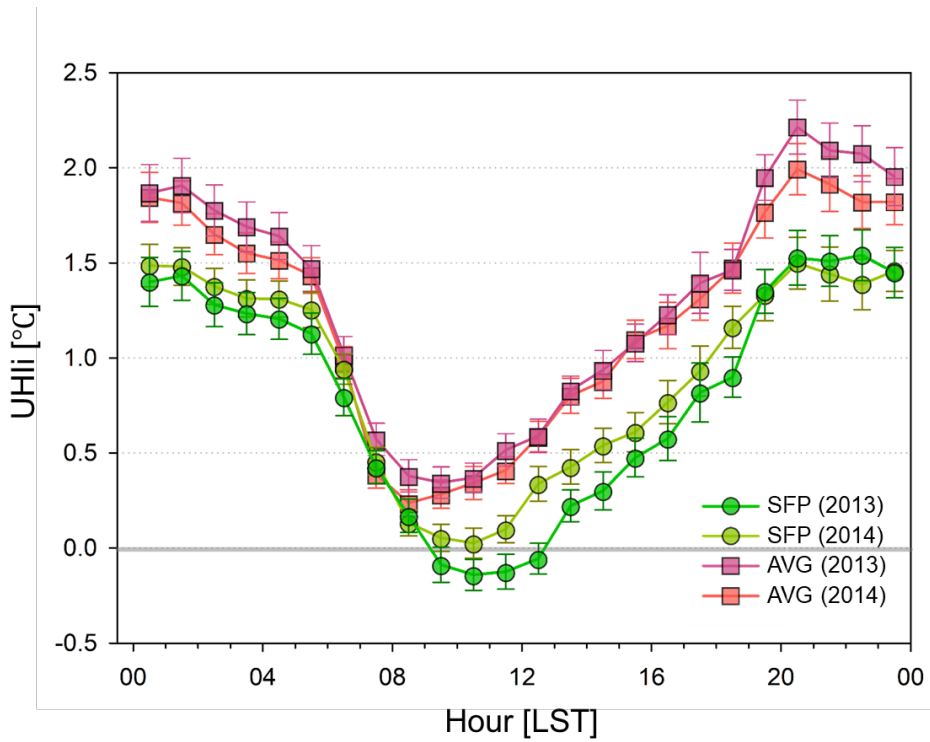
011 Figure 6. Hourly mean diurnal variation of the urban heat island intensity (UHI) of the SFP and CBD in the
 012 summer of 2013 and 2014. The error bars represent standard errors.

013



1014

1015 **Figure 7.** Mean diurnal pattern of air temperature difference (ΔT_{air}) between **AVG CBD** and **SD in summer** (a)
 1016 before and (b) after the construction of the park ~~in summer~~. **AVG CBD** indicates an average of three automatic
 1017 weather stations (Gangnam, Seocho, Songpa) in Seoul. The red dash line indicates the mean ΔT_{air} before and after
 1018 the construction of the park.

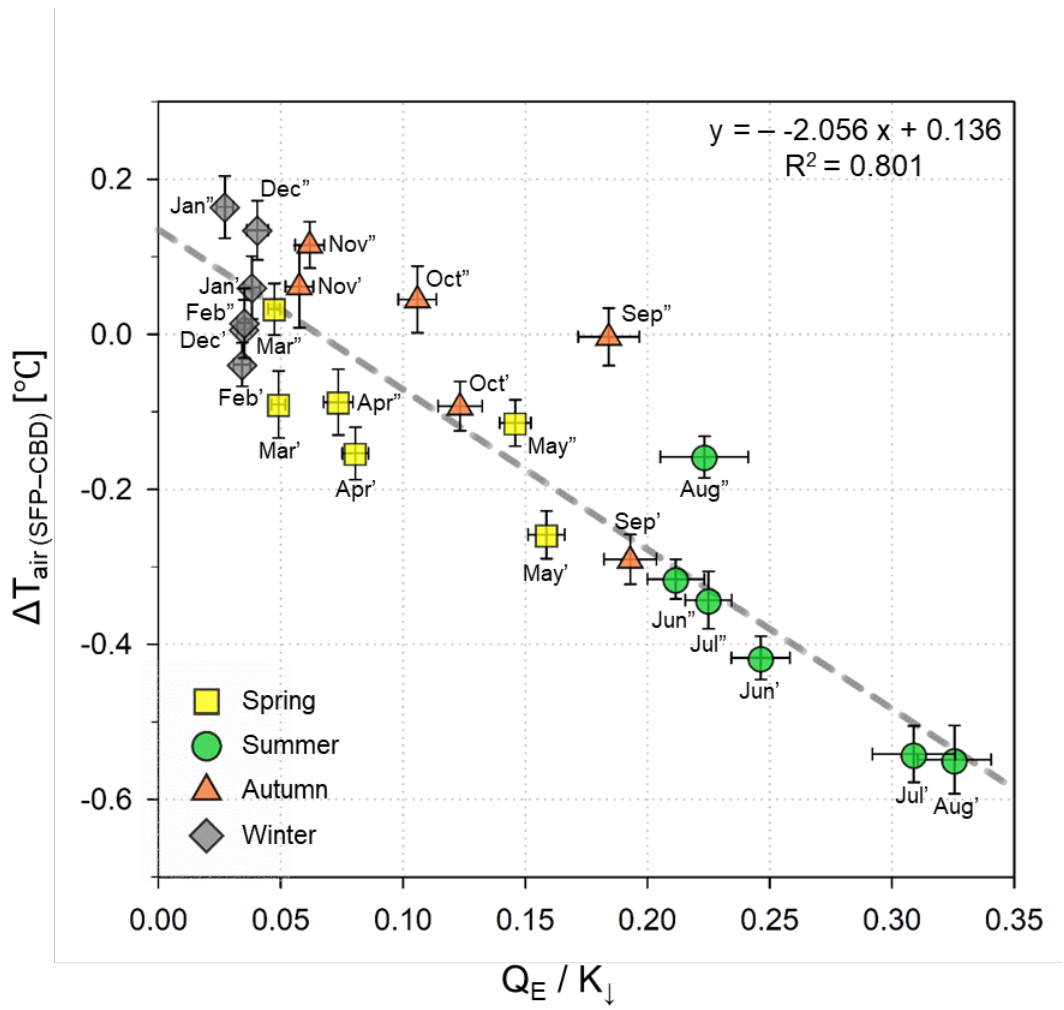


019

020

Figure 7. Hourly mean diurnal variation of the urban heat island intensity (UHli) of the SFP and AVG

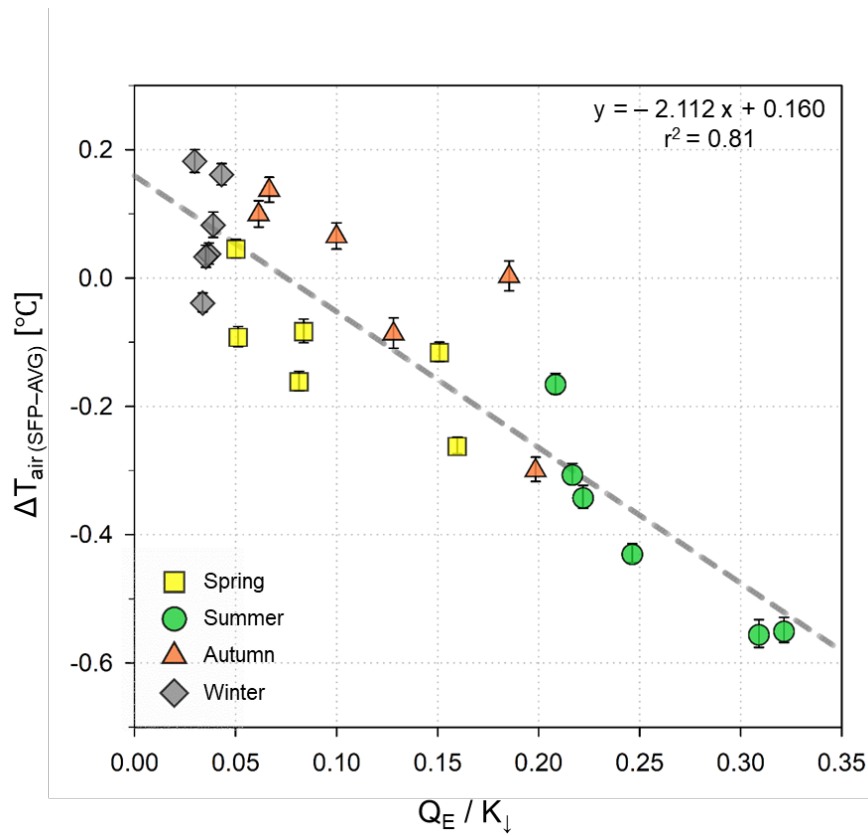
021
022



023
024
025

in the summer of 2013 and 2014. The error bars represent standard errors.

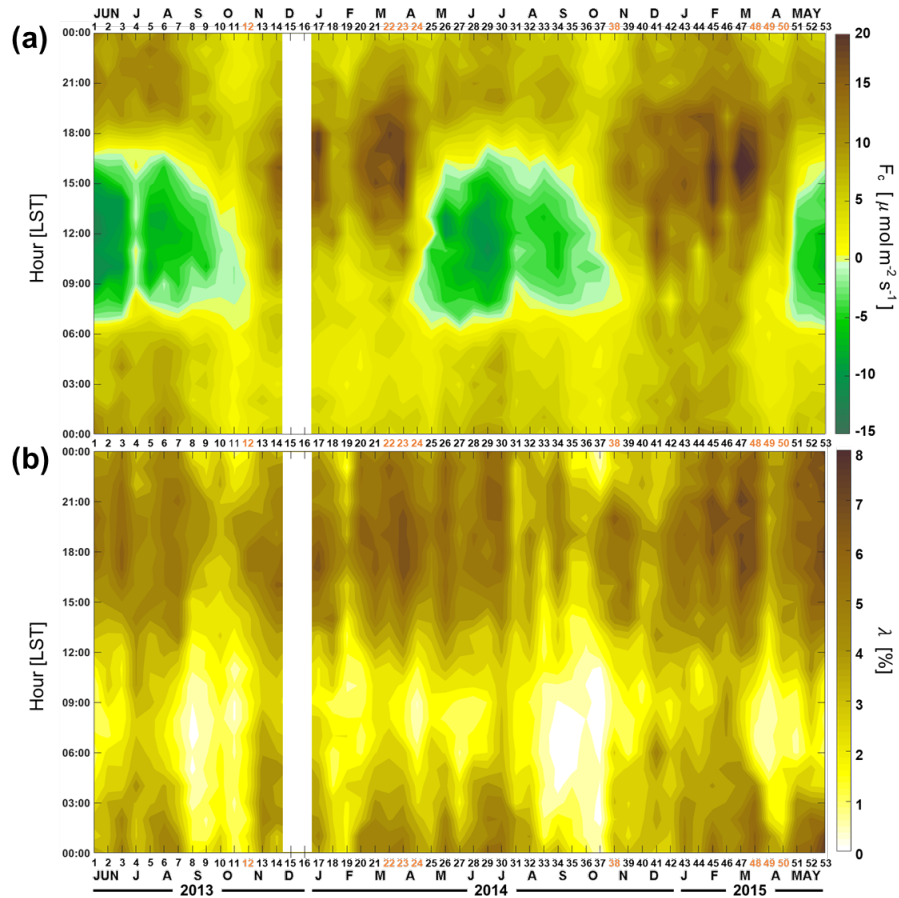
1026



1027

1028 Figure 8. Relationship between the ratio of monthly Q_E to K_{\downarrow} and mean air temperature difference between SFP
1029 and AVGCBD during the daytime ($K_{\downarrow} > 120 \text{ W m}^{-2}$) for two years. The quotation and double-quotation marks on
1030 the scatter indicate the first and second year of the observation period, respectively. The error bars represent
1031 standard errors based on daily values, and the grey dotted line is calculated using linear regression model
1032 considering errors in both axes (York et al., 2004).

1033



1035

1036

1037

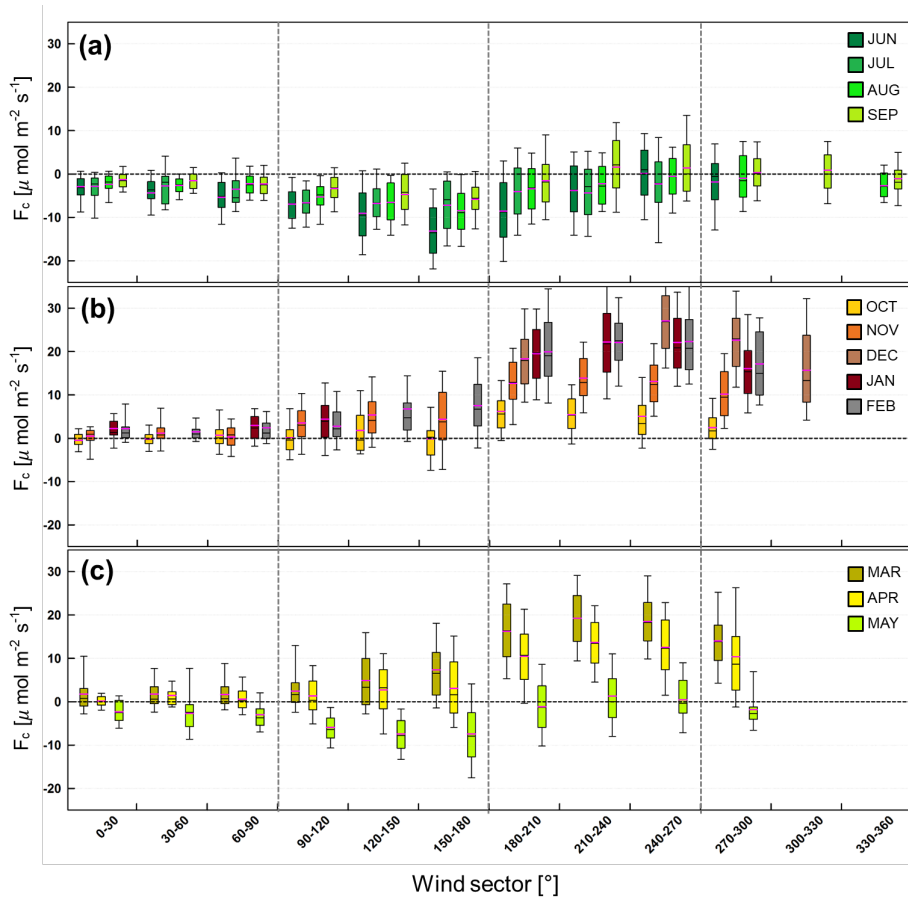
1038

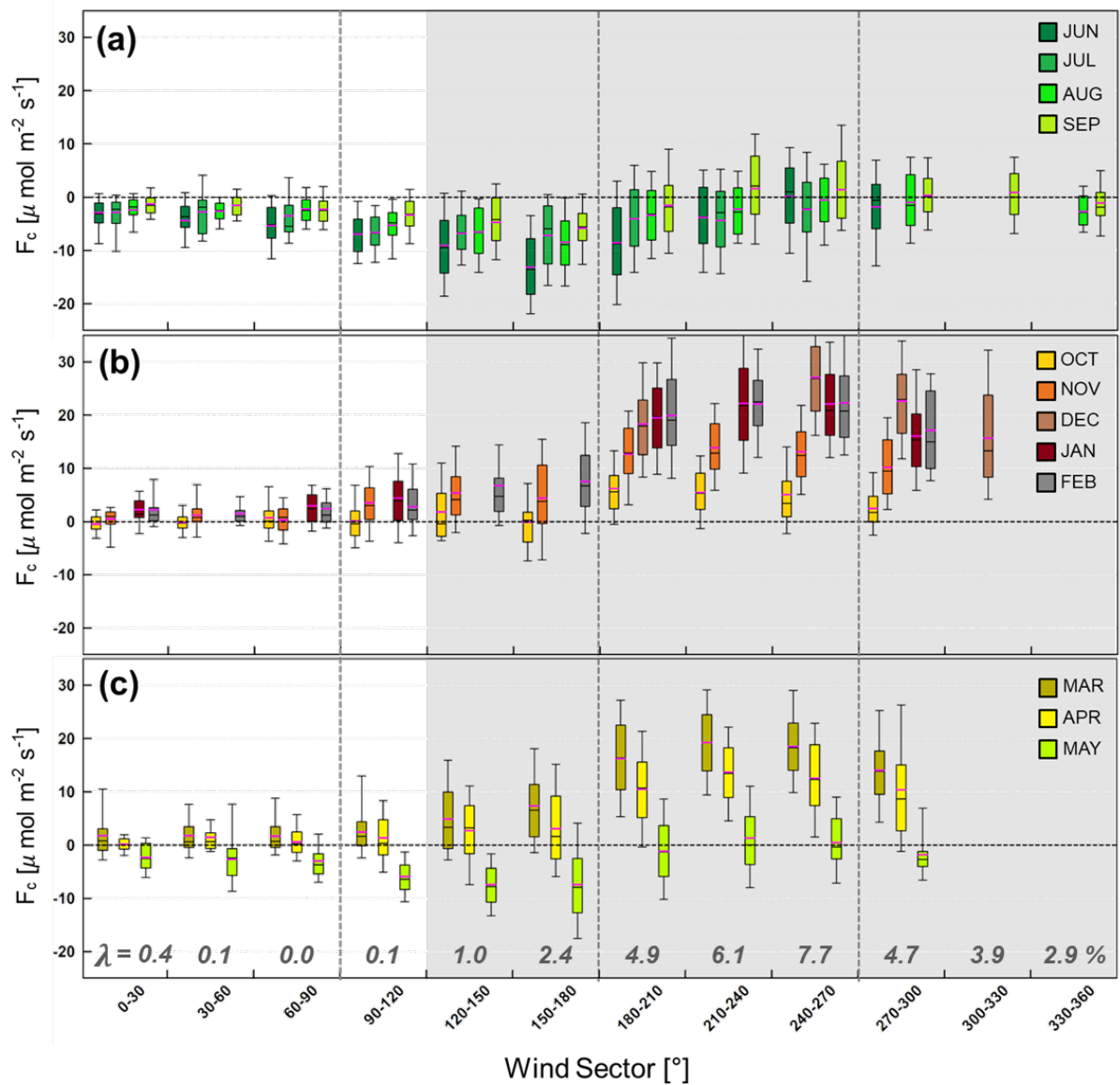
1039

1040

1041

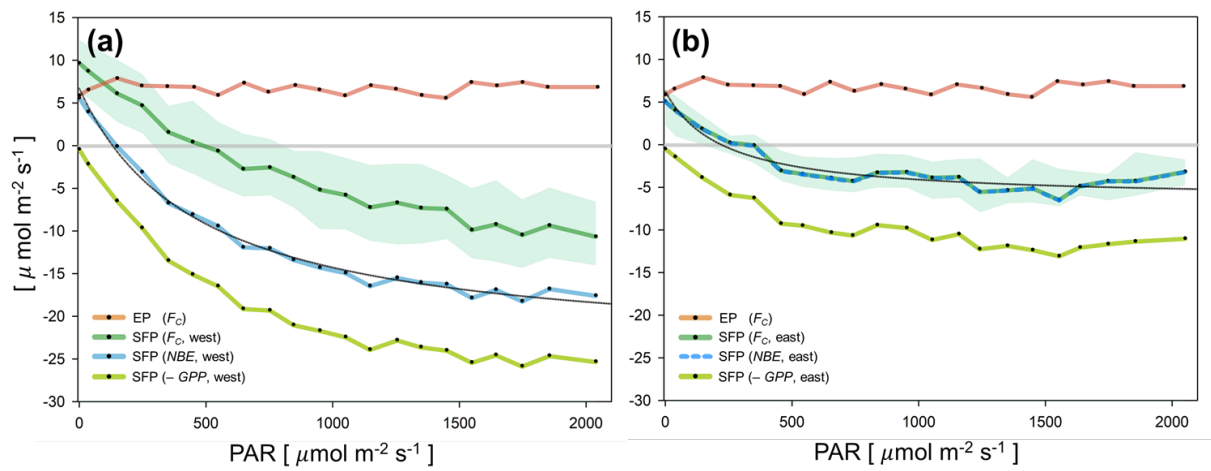
Figure 9. (a) Temporal variation of hourly averaged F_C and (b) source-area-footprint-weighted road fraction (λ) for as every two-week. The horizontal average (x-axis indicates: the order of every two-week for two years, and the vertical date, y-axis is the: time of day). In December 2013, there was a gap for approximately 4 weeks due to the power system failure. The yellow numbers in x-axis indicate the two-week (12th, 22nd-24th, 38th, and 48th-50th) having the transition period when the observed F_C is primarily attributable to traffic emissions (E_R). contributes to the observed F_C significantly.





1043

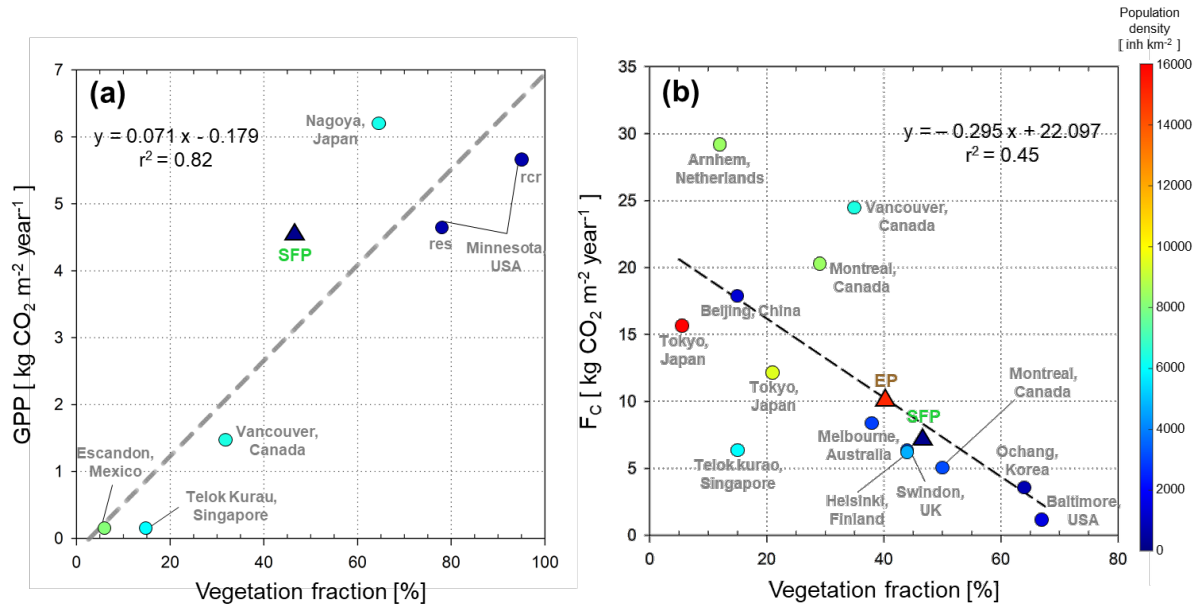
1044 Figure 10. Monthly boxplots of daytime ($K_t > 120 \text{ W m}^{-2}$) F_c by wind direction. Boxes have a minimum of 20
 1045 samples. Box limits are upper and lower quartiles, and whiskers are distances of 1.5 times the interquartile range
 1046 from each quartile. Median and mean values are indicated by the black and pink horizontal lines. The average
 1047 source area weighted road fractions (λ) are shown below the graph, and wind sectors with λ greater than 1% are
 1048 shaded in gray.



1049

1050 Figure 11. During the growing season (June–August 2013, 2014), when E_B is negligible, light-response curves
 1051 as a function of photosynthetically active radiation (PAR, in bins of $100 \mu\text{mol m}^{-2} \text{s}^{-1}$): (a) for the western sectors
 1052 ($150^\circ < \Phi < 300^\circ$) and (b) for the eastern sectors ($30^\circ < \Phi < 90^\circ$). Black line is a rectangular hyperbolic equation
 1053 fitting net biome exchange ($NBE = RE - GPP = F_C - E_R$) to PAR, and EP (brown line) is a light-response curve
 1054 for the high-rise high-population residential area in Seoul. The shaded areas indicate interquartile range.

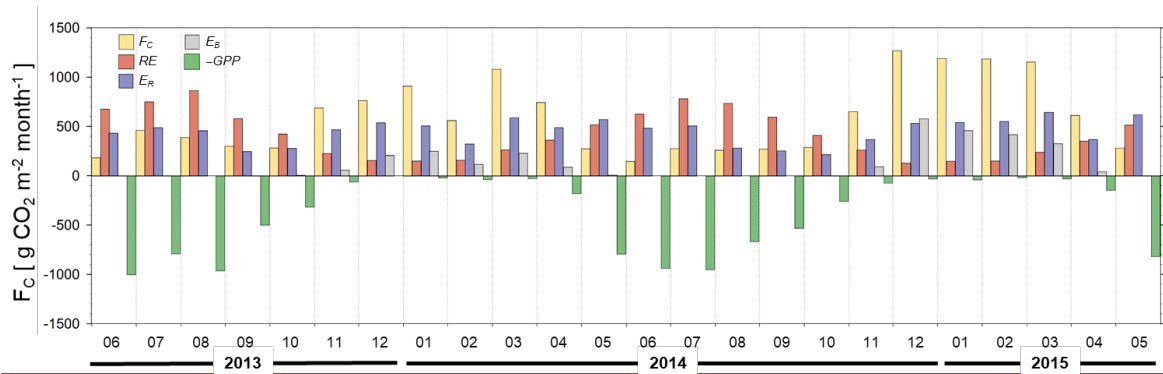
1055



1056
1057
1058
1059
1060
1061
1062

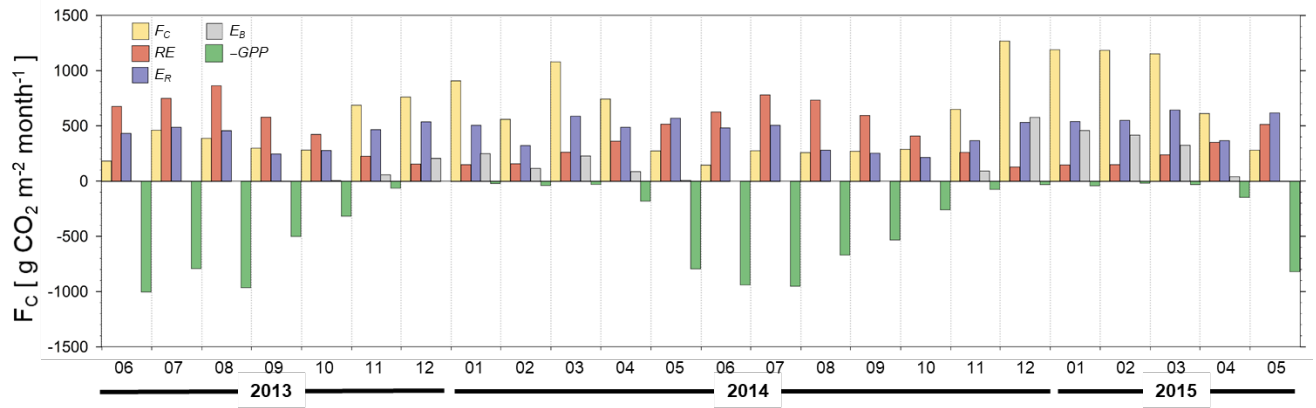
Figure 12. Relationship between vegetation fraction (a) annual *GPP* and (b) annual *F_c* in urban sites (Fig. 12a in Hong et al., 2019b). Dashed line in (a) and (b) indicates a linear regression of *GPP* in urban sites from Awal et al. (2010), Crawford and Christen (2015), Velasco et al. (2016), and Menzer and McFadden (2017) and *NEE* from Hong et al. (2019b) and references therein scaled with vegetation fraction, respectively. See main texts for more information.

063
064



065
066
067

1068



1069

1070

1071

Figure 13. Monthly sums for gap-filled F_c (yellow bar) with RE (red bar), E_R (blue bar), E_B (gray bar), and $-GPP$ (green bar)

1072

1073

